行政院國家科學委員會專題研究計畫 成果報告

以時變模式之行星齒輪系動態分析
研究成果報告(精簡版)

計 畫 類 別 ：個別型
計 畫 編 號 ：NSC 95-2221-E-216-008-
執 行 期 間 ：95 年 08 月 01 日至 96 年 09 月 30 日
執 行 單 位 ：中華大學機械工程學系

計 畫 主 持 人：黃國饒

計畫參與人員：碩士級兼任助理：陳建羽、陳志傑

報 告 附 件 ：出席國際會議研究心得報告及發表論文

處 理 方 式 ：本計畫可公開查詢

中 華 民 國 96 年 12 月 24 日

行政院國家科學委員會補助專題研究計畫 ■ 成 果 報 告 □期中進度報告

（以時變模式之行星齒輪系動態分析）

計畫類別：■ 個別型計畫　　□ 整合型計畫
計畫編號：NSC－95－ 2221－ E－216－ 008
執行期間：　95　年　8　月　1　日至　96　年　9　月　30　日

計畫主持人：黃 國 饒
共同主持人：
計畫參與人員：陳建羽、陳志傑

成果報告類型(依經費核定清單規定繳交)：■精簡報告　□完整報告

本成果報告包括以下應繳交之附件：
□赴國外出差或研習心得報告一份
□赴大陸地區出差或研習心得報告一份
■出席國際學術會議心得報告及發表之論文各一份
□國際合作研究計畫國外研究報告書一份

處理方式：除產學合作研究計畫、提升產業技術及人才培育研究計畫、列管計畫及下列情形者外，得立即公開查詢
□涉及專利或其他智慧財產權，□一年□二年後可公開查詢

執行單位：中華大學機械系

中　華　民　國　96　年　12　月　20　日

中文摘要

本計畫建立兩種時變模式的行星齒輪系動態分析方法，包括應用等效離散與連體幾何模式，兩者動態結果將互相比較以瞭解理論模式與數值結果的正確性。在離散模式方面，以Lagrange方程式推導出離散模式行星齒輪系之運動方程式。考慮漸開線齒輪嚙合關係，計算出嚙合點與嚙合齒對數目的變化以及齒對嚙合相位關係來獲得外、內齒輪對之等效時變嚙合剛度。再以Jacobi 轉換與朗吉-庫塔法，計算行星齒輪系的自然頻率與動態齒根應力。在連體模式方面，為了精確描述輪齒外形並減少數值計算時間，直接應用所推導的齒輪幾何外形方程式，產生高品質且易調整密度與數量的網格元素模型。以進行連體幾何時變模式的行星齒輪系動態分析。最後進行設計參數分析，討論齒輪中心距與背隙、齒頂修整、轉速與負載等條件其對於行星齒輪系動態特性之影響。本計畫已增強國內行星齒輪系統動態分析與設計之基礎。

關鍵字：行星齒輪系，動態分析，嚙合相位，有限元素，動態嚙合力，動態齒根應力、LS-DYNA

英文摘要

This project develops two approaches of the time varying models to analyzing dynamics for an involute planetary gear system, that are respectively using a discrete model and a continuous geometry model by the finite element method. In the discrete approach, numbers, positions, phasing differences of the meshing tooth pairs are described by time varying and nonlinear meshing stiffnesses. Natural frequencies, meshing forces, fillet stresses, and dynamic factors can be calculated by using the Jacobi transformation and the Runge-Kutta integration. In the continuum approach, dynamics of the planetary gear system are analyzed using the software, LS-DYNA. The approach of the continuous geometry model can incorporate the time varying properties intrinsically. In this continuum study, high quality mesh elements of the planetary gear system are automatically generated directly using the derived tooth profile equations. After assigning initial and boundary conditions, dynamic responses for the planetary gear system are solved. Fillet stresses resulting from the both approaches are verified by each other comparisons. Finally, the parametric analysis is performed to investigate the influences of center distances, backlashes, modification, rotation speeds, and loadings on the dynamics. The results are expected to enhance analysis and design ability for the planetary gearings.

Keywords: Planetary gear system, Dynamic analysis, Meshing phase, Finite element, Dynamic contact force, Dynamic fillet stress, LS-DYNA

1. 前言

齒輪系統具有傳動確實、精密、效率高以及體積小等優點，一直為機械傳動最重要的組件。其中行星齒輪系更由於具有低振動噪音、高功率體積比、高減速比以及易達成輸出入軸同心軸之設計等特性，在各種高精密與高速度產業與機械所廣泛採用。為了滿足上述產業發展更嚴格的要求，降低振動噪音增加運轉精度與壽命，對於行星齒輪系統動態特性之研究，已日漸成為重要的課題。

2. 研究目的

影響行星齒輪系的動態之參數極多，而其中應用齒頂移位的技術，可以調整齒輪中心距、嚙合背隙與齒數、防止過切、以及嚙合剛性與嚙合相位等設計條件，是改善動態特性的最重要方法。但關於齒頂移位對於行星齒輪系動態之影響，則仍未被討論，本計畫將予以探討之，希望計畫成果可作為國內行星齒輪系統設計之參考。

3. 文獻探討

事實上很早即有學者開始進行行星齒輪系統的動態特性研究[1]，Kahraman [2]則以四個等間距分佈行星齒輪，考慮嚙合相位變化以及齒形誤差造成之激振源，最早分析螺旋行星齒輪系統之振動模態，並且予以分類；而Parker [3]則以二維模式進一步分析包括三個與四個行星齒輪的行星齒輪系，探討考慮嚙合相位對於動態特性之影響。根據Velex 和 Flamand [4]的研究，指出齒對之嚙合剛度對於行星齒輪系動態之影響比太陽齒與環齒輪之軸與軸承支撐剛度影響大。Lin和Parker[5]則以離散模式計算行星齒輪系統之各個自然頻率，討論由於剛度不連續之非線性現象，產生諧波共振特性。同作者[6]則計算行星齒輪系統之自然頻率與重疊個數，並將其振動模態分為旋轉、平移與行星齒輪三種模式來進行討論。但是上述簡化等效離散模式，僅能分析極為簡化之齒輪系種類與條件。

隨著電腦輔助工程技術發展已日趨成熟，齒輪力學分析已逐漸由簡化的等效離散模式進展至以有限元素法之連體方法來處理齒輪系靜動態問題。關於行星齒輪系方面，最近Yuksel和Kahraman [7]則以有限元素法，分析齒輪磨耗量，並且討論磨耗量對於行星齒輪系動態特性之影響，指出太陽齒輪磨耗量最大，而且此磨耗對於齒輪系統頻率模態之動態嚙合力影響最明顯；而Bajer和Demkowicz [8]則是最早利用多體模式與接觸理論，同時考慮剛體與撓性體影響，分析行星齒輪系統的衝擊與總能量之變化。最近Litvin等學者[9]研究將行星齒輪同時施以齒形與導程修整，進行行星齒輪系之輪齒接觸分析，希望減少其傳動誤差與振動；然而目前此種連續體幾何模式的分析方法，基本上仍只著重於靜態力學分析為主，直到最近的研究 [10]才開始直接應用近連體模式之有限元素方法來進行齒輪動態問題之探討。

4. 研究方法

4.1 理論離散模式

4.1.1 運動方程式

圖1(a) 是本文所探討的行星式正齒輪系之實體模型，將其環齒輪固定於齒輪箱體不動，以太陽齒輪為輸入端，行星架為輸出端，圖1(b)則為二維等效離散模式圖示。以 Lagrange方程式推導出行星式齒輪系統的運動方程式，並且先做以下假設：1. 以二維模式來描述正齒輪之行星齒輪系統，2. 齒輪對嚙合關係以等效平移彈簧相切連接於兩齒輪之基圓來描述，3. 軸承效用以等效平移彈簧模擬，而輸出入軸以等效旋轉彈簧模擬，4. 忽略齒輪與其他元件之製造誤差，5. 忽略行星架的彈性旋轉變形對行星齒輪動能的影響。以下將太陽齒輪-行星齒輪之外齒輪對簡稱為外齒輪對，而環齒輪-行星齒輪之內齒輪對簡稱為內齒輪對。首先推導行星齒輪系統各構成組件之動能與彈性位能於第 (1)~(13)式。

動能方程式：

$$T^{(d)}=\frac{1}{2}J^{(d)}\left(n^{(d)}+\dot{\phi}^{(d)}\right)^2 \quad (1)$$

$$T^{(s)}=\frac{1}{2}J^{(s)}\left(n^{(s)}+\dot{\phi}^{(s)}\right)^2+\frac{1}{2}m^{(s)}\left[\left(\dot{x}^{(s)}\right)^2+\left(\dot{y}^{(s)}\right)^2\right] \quad (2)$$

$$T^{(i)} = \sum \frac{1}{2} J^{(i)} \left(n^{(i)} + \dot{\phi}^{(i)} \right)^2 + \sum \frac{1}{2} m^{(i)} \left[\left(-r_b^{(c)} n^{(c)} \sin \Psi_i + \dot{x}^{(i)} \right)^2 + \left(r_b^{(c)} n^{(c)} \cos \Psi_i + \dot{y}^{(i)} \right)^2 \right] \tag{3}$$

$$T^{(c)} = \frac{1}{2} J^{(c)} \left(n^{(c)} + \dot{\phi}^{(c)} \right)^2 \tag{4}$$

$$T^{(r)} = \frac{1}{2} J^{(r)} \left(n^{(r)} + \dot{\phi}^{(r)} \right)^2 + \frac{1}{2} m^{(r)} \left[\left(\dot{x}^{(r)} \right)^2 + \left(\dot{y}^{(r)} \right)^2 \right] \tag{5}$$

$$T^{(o)} = \frac{1}{2} J^{(o)} \left(n^{(o)} + \dot{\phi}^{(o)} \right)^2 \tag{6}$$

位能方程式：

$$V^{(ds)} = \frac{1}{2} k^{(ds)} \left(\phi^{(d)} - \phi^{(s)} \right)^2 \tag{7}$$

$$V^{(s)} = \frac{1}{2} k^{(sx)} \left(x^{(s)} \right)^2 + \frac{1}{2} k^{(sy)} \left(y^{(s)} \right)^2 \tag{8}$$

$$V^{(si)} = \frac{1}{2} k^{(si)} \left(d^{(si)} - E^{(si)} \right)^2 \tag{9}$$

$$V^{(ri)} = \frac{1}{2} k^{(ri)} \left(d^{(ri)} - E^{(ri)} \right)^2 \tag{10}$$

$$V^{(c)} = \sum_i \frac{1}{2} k^{(cix)} \left(x^{(i)} + r_b^{(c)} \phi^{(c)} \sin \Psi_i \right)^2 + \sum_i \frac{1}{2} k^{(ciy)} \left(y^{(i)} - r_b^{(c)} \phi^{(c)} \cos \Psi_i \right)^2 \tag{11}$$

$$V^{(r)} = \frac{1}{2} k^{(rx)} \left(x^{(r)} \right)^2 + \frac{1}{2} k^{(ry)} \left(y^{(r)} \right)^2 \tag{12}$$

$$V^{(oc)} = \frac{1}{2} k^{(oc)} \left(\phi^{(o)} - \phi^{(c)} \right)^2 \tag{13}$$

其中$T^{(*)}$和$V^{(*)}$是動能和彈性位能、$J^{(*)}$：慣性矩，$m^{(*)}$：質量，$n^{(*)}$和$\dot{\phi}^{(*)}$：各元件剛體與彈性變形之轉度，$\dot{x}^{(*)}$和$\dot{y}^{(*)}$：彈性變形之平移速度。上標符號 * 可以為 d，s，c，p，r，o 將分別代表輸入軸、太陽齒輪、行星齒輪、行星架、環齒輪和輸出軸；i為第i個行星齒輪。$V^{(d)}$是輸入軸的位能，$V^{(s)}$是太陽齒輪平移的彈性位能，$V^{(si)}$是第i個行星齒輪和太陽齒輪間的位能，$V^{(ri)}$是行星齒輪和環形齒輪間的位能，$V^{(ci)}$是行星齒輪和齒輪架間之彈性位能，$V^{(r)}$是環齒輪的平移彈性位能，$V^{(oc)}$是輸出軸的位能，而$r_b^{(*)}$與$r_a^{(*)}$則為齒輪基圓與齒項圓半徑。

另外$d^{(si)}$與$d^{(ri)}$則代表第i個行星齒輪分別與太陽齒輪和環齒輪在作用線方向的相對位移，而$E^{(si)}$與$E^{(ri)}$則為其誤差

將(1)~(13)式代入Lagrange方程式，並包含阻尼模式效應，可得離散模式之正齒輪系統的運動方程式

$$\mathbf{M}\ddot{\mathbf{x}} + \mathbf{C}\dot{\mathbf{x}} + \mathbf{K}\mathbf{x} = \mathbf{F} \tag{14}$$

其中**M**為質量矩陣、**C**阻尼矩陣、**K**剛度矩陣、**x**位移向量與**F**外力向量，詳細推導內容與各矩陣之元素可參考[11]。而齒對等效時變嚙合剛度與相位關係之推導則說明於以下二節中。

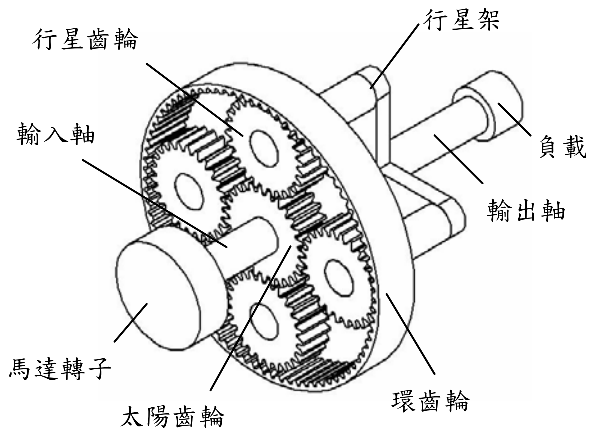

(a) 實體模型

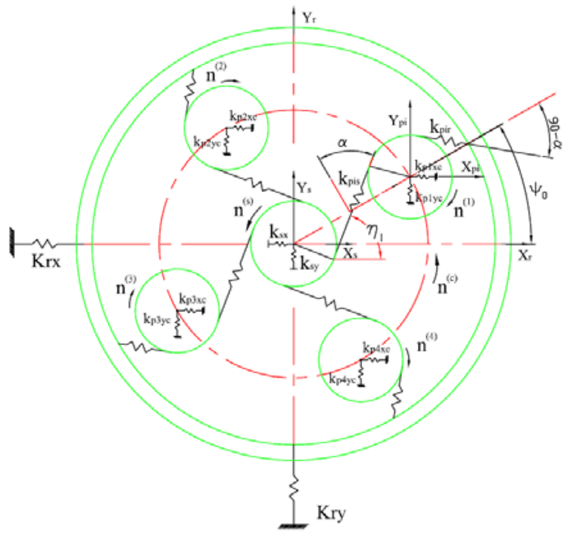

(b) 2D等效離散物理模式

圖1 行星齒輪系統之實體與物理模式

4.1.2 齒對嚙合剛度

本研究齒輪對之等效時變嚙合剛度是採用Kuang和Yu [12]研究結果來計算。齒輪對的總體嚙合剛度包括輪齒承受彎矩之可撓度q_{Tj}，輪齒與本體彈性支承之局部變形的可撓度 q_{Bj} 以及嚙合齒對以赫茲接觸理論計算之瞬間接觸變形可撓度 q_{Hj}，所以嚙合齒輪對的第j對嚙合輪齒對剛度$k_{pg,j}$可表示為

$$k_{pg,j} = (q_{Tj} + q_{Bj} + q_{Hj})^{-1} \tag{15}$$

考慮齒輪嚙合過程之齒對數目的時變特性，所以齒輪 p、g 構成之齒輪對嚙合剛度可寫成

$$k_{pg} = \sum_{j=1}^{n_T} k_{pg,j} \tag{16}$$

(16)式中 n_T 為嚙合齒對的數目通常為1 或2。

4.1.3 齒輪對嚙合相位差關係

圖2與圖3表示各種齒輪對之角度分佈關係，圖中的點 C_i 、$\mathrm{C}_i^{'}$ 分別代表為外、內齒輪對接觸點，P_i 、$\mathrm{P}_i^{'}$ 為接觸節點，$r_a^{(*)}$ 與 $r_b^{(*)}$ 分別為齒頂圓與齒底圓半徑，上標符號*可以為 s，p，r將分別代表太陽齒輪、行星齒輪與環齒輪，而 r_{C_i} 為接觸點半徑，$z^{(s)}$、 $z^{(r)}$ 為齒數，$\psi_c^{(k)}$ 為第1個行星齒輪與第 k 個行星齒輪之相隔角度，$2\pi / z^{(s)}$ 、$2\pi / z^{(r)}$ 為太陽齒輪與環齒輪的分配角。而各種齒輪對嚙合相位之間的關係推導於下。

(一)第 k 組外齒輪對與第 1 組外齒輪對間之相位差

假設第1組外齒輪對在節點 P_1 嚙合，所以第1個行星齒輪與第 k 個行星齒輪間相隔之太陽齒輪分配角的個數為

$$\frac{\psi_c^{(k)}}{2\pi / z^{(s)}} \quad 或 \quad \frac{\psi_c^{(k)} \cdot z^{(s)}}{2\pi} \tag{17}$$

(a) 若 (17)式可整除，即

$$\frac{\psi_c^{(k)} \cdot z^{(s)}}{2\pi} = \mathrm{int}(\frac{\psi_c^{(k)} \cdot z^{(s)}}{2\pi})$$

則第 k 輪組與第 1 組外齒輪對間無相位差， int 表示取整數。

(b) 若(17)式不可整除，則第 k 組行星齒輪與第1個行星齒輪相隔於太陽齒輪齒數(分配角度)的數目為

$$n^{(s)} = \mathrm{int}(\frac{\psi_c^{(k)} \cdot z^{(s)}}{2\pi} + 1) \tag{18}$$

而且第 k 組外齒輪對與第 1 組外齒輪對之間存有嚙合相位差。此相位差值推導於下，首先由圖(2) 第 k 組太陽齒輪漸開線起點與連心線 $\overline{O_{pk}O_s}$ 之夾角為

$$\theta_1 = \frac{2\pi \cdot n^{(s)}}{z^{(s)}} - \psi_c^{(k)} + \mathrm{inv}\alpha_{sp} \tag{19}$$

上式之 inv 為漸開線函數。所以可得到第 k 組外齒輪對與第 1 組外齒輪對之相位差 $\kappa_{sp}^{(k)}$ 為：

(i) 當 $\mathrm{r}_{\mathrm{C}_k} \geq r_a^{(s)}$ ，則相位差 $\kappa_{sp}^{(k)} = \theta_1 - \frac{2\pi}{z^{(s)}} - \mathrm{inv}\alpha_{sp}$

(ii) 當 $\mathrm{r}_{\mathrm{C}_k} < r_a^{(s)}$ ，其相位差 $\kappa_{sp}^{(k)} = \theta_1 - \mathrm{inv}\alpha_{sp}$

而且，若 $\kappa_{sp}^{(k)} > 0$ 則第 k 組外齒輪對領先第 1 組外齒輪對；而若 $\kappa_{sp}^{(k)} < 0$ 則第 k 組外齒輪對則是落後第 1 組外齒輪對。同樣的方法，可得到 第 k 組內齒輪對與第 1 組內齒輪對間之相位差。

(二) 第 1 組內齒輪對與第 1 組外齒輪對間之相位差

應用圖 3 推導內、外齒對間嚙合相位關係，先假設第1組外齒輪對在節點 P_1 嚙合，而 κ_{sr} 為第 1 組內齒輪對與第 1 組外齒輪對間之相位差。由圖 3所示，第 1 組外齒輪對之行星齒輪漸開線起點與連心線 $\overline{O_1O_s}$ 之夾角為

$$\beta_{p1} = \mathrm{inv}\alpha_{sp} \tag{20}$$

所行星齒輪之另一邊漸開線基圓起點與 $\overline{O_1O_s}$ 之夾角為

$$\theta_3 = \frac{t_p}{r_b^{(p)}} + 2\mathrm{inv}\alpha_0 - \beta_{p1} \tag{21}$$

上式中 α_0 是刀具壓力角，而 t_p 為節圓齒厚，可寫成

$$t_p = \pi m / 2 + 2e\tan\alpha_0 \tag{22}$$

其中 m 為模數，e 為移位量。所以，

$$\theta_3 = \frac{\pi}{z^{(s)}} + \frac{2e\tan\alpha_0}{mz^{(s)}} + 2\mathrm{inv}\alpha_0 - \mathrm{inv}\alpha_{sp} \tag{23}$$

然後找出此行星齒輪與內齒輪嚙合且第一個超過連心線之輪齒，其跨過的分配角度個數 n_1 ，將可以用(24)式來判斷

$$\frac{\pi - \theta_3}{2\pi / z^{(p)}} \tag{24}$$

(a) 若 (24)式可整除， $n_1 = (\pi - \theta_3)/(2\pi / z^{(p)})$

(b) 若不可整除，則 $n_1 = \mathrm{int}[(\pi-\theta_3)/(2\pi/z^{(p)})+1]$
因此，行星齒輪漸開線起點與連心線 $\overline{O_1O_s}$ 之夾角 κ_1 為

$$\kappa_1 = n_1 \cdot \frac{2\pi}{z^{(p)}} + \theta_3 - \pi \tag{25}$$

使用 $\overline{ED} = \widehat{EC}$ 之關係可得到

$$\theta_4 = \tan^{-1}(\alpha_{rp} + \kappa_1) \tag{26}$$

最後第 1 組內齒輪對與第 1 組外齒輪對角度 κ_{sr} 即為

$$\kappa_{sr} = \mathrm{inv}\theta_4 - \mathrm{inv}\alpha_{rp} \tag{27}$$

(i) 當 $\kappa_{sr} > 0$，則第 1 組內齒輪對嚙合會超前第 1 組 外齒輪對 κ_{sr} 角度。

(ii) 當 $\kappa_{sr} < 0$，則第 1 組內齒輪對嚙合會落後第 1 組 外齒輪對 $-\kappa_{sr}$ 角度。

最後應用上述三種齒輪對之相位差關係，可獲得行星齒輪系統中任何兩組齒對間的瞬間嚙合相位差的關係。

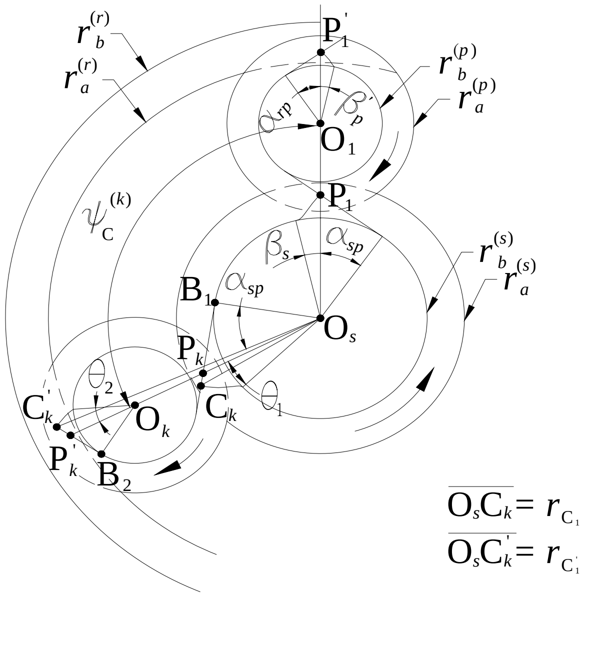

圖2 第 k 組與第 1 組的外齒輪對以及內齒輪對的嚙合相位關係

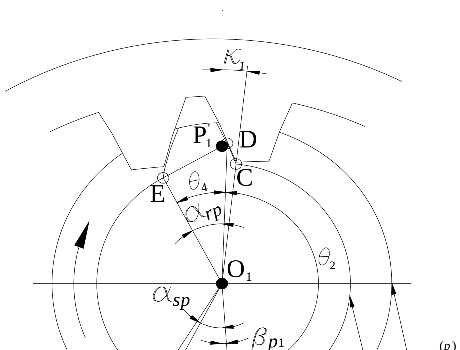

圖3 第 1 組內齒輪對與第 1 組外齒輪對間的嚙合相位關係

4.1.4 以離散模式的動態分析

應用前兩節討論之行星齒輪系架構與齒輪間嚙合關係，計算出各齒輪對之嚙合點位置、嚙合齒對數目以及相位關係，先獲得太陽齒輪-行星齒輪與環齒輪-行星齒輪之等效時變齒輪對嚙合剛度，再代入(17)之行星齒輪系運動方程式。設定輸出入軸施以傳動扭矩，以 Jacobi 轉換計算行星齒輪系的自然頻率，並以朗吉-庫塔法計算其動態嚙合力、齒根應力以及動態因子。而動態因子在此則定義為動態嚙合力與靜態嚙合力之比值。

4.2 LS-DYNA 的動態分析

4.2.1 行星齒輪系之有限元素模型

所分析的行星齒輪系統是由漸開線標準齒輪所組成，齒輪系之有限元素模型建立先以齒條形刀具截面方程式，經由HTM與齒輪嚙合方程式[13]創成出漸開線齒輪理論外形，直接應用所推導的齒輪理論模式，產生高品質且易調整密度與分佈的網格元素，以減少網格元素數量與數值計算時間。圖4為本研究所分析之齒輪系之網格模式，其齒輪參數如下：模數1.5mm，壓力角 $\alpha_0 = 20^\circ$ 齒數:太陽齒輪 $z^{(s)} = 28$、行星齒 $z^{(p)} = 28$、環齒輪 $z^{(r)} = 84$。圖中所有支撐軸承以等效支撐彈簧來描述之。

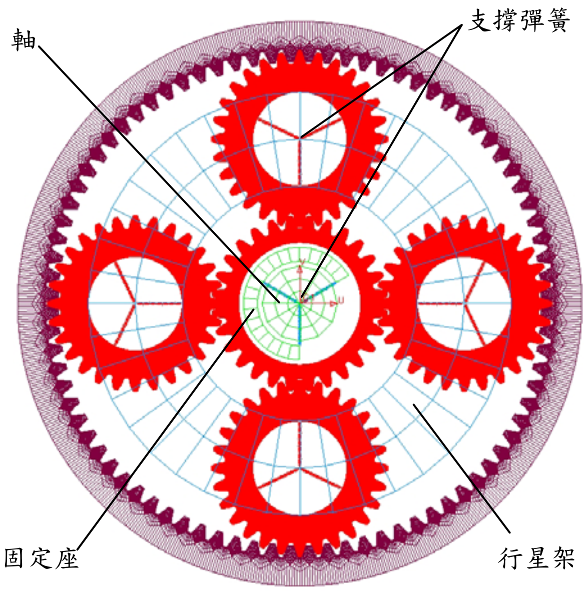

圖4 行星齒輪系統的有限元素網格模型

4.2.2 LS-DYNA設定

將完整的行星齒輪系統有限元素模型，設定所需材料參數與模型元素特性。在此所有元件材料皆設定為鋼材；太陽齒輪與行星齒輪為線性彈性材料，但不考慮行星齒輪軸部變形的影響，因此設定行星齒輪軸部性質為剛體材料；環齒輪因為固定於箱體，相對於其它齒輪的變形量很小，所以設定為剛體材料。此外不考慮輸入軸、輸出軸、固定座、行星架等元件之彈性變形的影響，以上材質皆設定為剛體。然後建立各齒輪對間的元件接觸條件與限制關係。將輸入軸與輸出軸分別與太陽齒輪與行星架做連接設定。再設定扭矩於輸入軸與轉速於輸出軸，以及初始條件設定輸出、入軸的轉速等。然後給定數值模擬時間與輸出條件，最後載入LS-DYNA求解器進行行星齒輪系動態模擬。

5. 結果與討論

5.1 離散模式結果與討論

5.1.1 齒對嚙合剛度

首先計算齒輪對於嚙合週期過程中，內外齒輪對之嚙合剛度變化。圖5中外齒輪對之嚙合剛度，在初始嚙合時其嚙合剛度為 3.63×10^8 N/m ，此時正值雙齒對嚙合，嚙合齒對的數目為二，當嚙合角度達 4.7° 時嚙合剛度為最大值之 3.87×10^8 N/m ，嚙合角度到 8.2° 時，由於前一齒對嚙合已結束，所以此時嚙合狀態為單齒嚙合，到 12.9° 時再恢復雙齒對嚙合，直到 21.1° 嚙合結束。在嚙合角度為 4.7° 與 17.6° 時出現嚙合過程中剛度最大值 3.87×10^8 N/m ，此時為雙齒對嚙合。而單齒對之嚙合剛度最大值出現在節點位置接觸之 10.8° 的 2.19×10^8 N/m 。齒對嚙合剛度變化，從開始嚙合至結束之過程則呈現左右對稱分佈。圖5也表示內齒對在一嚙合週期過中嚙合剛度隨嚙合角度改變，圖中可顯示出內外齒對間嚙合相位。

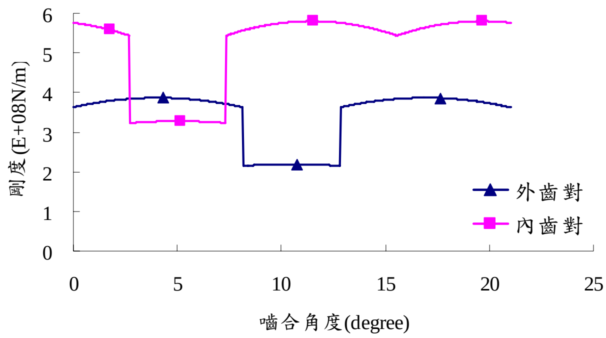

圖5 內外齒對嚙合剛度變化

5.1.2 離散模式動態嚙合力

圖6(a)、6(b)分別為太陽齒輪轉速2000 rpm，阻尼比0.075，太陽齒與四個行星齒輪和環齒輪與四個行星齒輪嚙合時，動態嚙合力隨嚙合角度之變化情形。以下討論圖6(a)中太陽齒輪與第1、3行星齒輪之動態嚙合力與嚙合角度之關係，在嚙合初期，嚙合狀態為兩齒對嚙合．其動態嚙合力為131 N，隨著嚙合角度的增加，動態嚙合力呈現增大現象；當嚙合角度達 12.3° 時，此時前一齒對嚙合剛結束，外齒輪對由兩齒對轉為單齒對嚙合，所以動態嚙合力出現急遽增大現象，而在嚙合角 $12.3^\circ\sim17.1^\circ$ 期間一直維持單齒嚙合狀態，所以此期間動態嚙合力都維持較大值；直到 17.1° 時，下一組嚙合齒對開始進入嚙合，嚙合狀態恢復為兩齒對嚙合，因此動態嚙合力快速的減小，直到 27.8° 整個嚙合過程結束。結果顯示動態嚙合力的變化與嚙合齒對數目改變有最直接關係。此外圖6(a)也顯示第1、3太陽齒與行星齒輪間的動態嚙合力以及第2、4太陽齒與行星齒輪間的動態嚙合力數值與變化，

各呈現完全相同現象，而第1、3與第2、4行星齒輪之間動態嚙合力數值則稍有不同，但變化趨勢則極相近為何有差異。圖6(b)為環齒輪與四個行星齒輪之動態嚙合力與嚙合角度之變化關係，與外齒輪對間則存有相位差，但變化趨勢與外齒輪對相似，其動態嚙合力與嚙合齒對個數有最直接的影響關係。

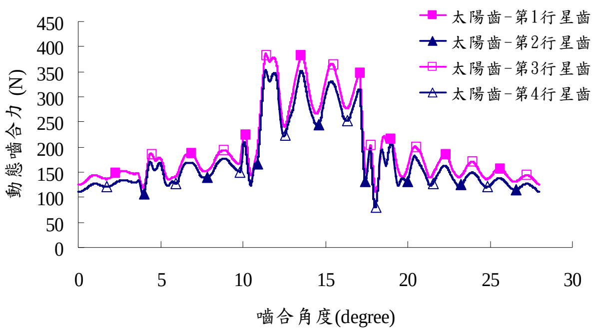

(a) 太陽齒與四個行星齒嚙合之動態嚙合力

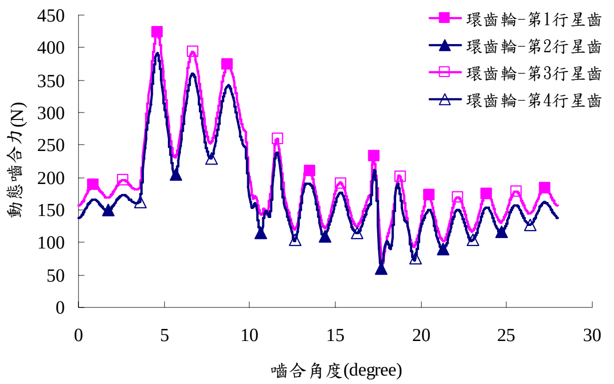

(b) 環齒輪與四個行星齒嚙合之動態嚙合力

圖6行星齒輪系在一嚙合週期之動態嚙合力

5.1.3 離散模式動態齒根應力

以下以離散模式分析先獲得外齒輪對的動態嚙合力，再以路易士公式計算出行星齒輪之動齒根應力。圖7即為輸入軸轉速分別是2000rpm、4000rpm、6000rpm、8000rpm與10000rpm，輸入軸傳遞扭矩150N-m，阻尼比0.075，太陽齒與行星齒輪嚙合時，動態齒根應力隨嚙合角度之變化情形。以下討論圖7中2000 rpm時太陽齒輪與行星齒輪之動態齒根應力與嚙合角度之關係；在嚙合初期，嚙合狀態為兩齒對嚙合·隨著嚙合角度的增加，動態齒根應力呈現慢慢增大的現象；當嚙合角度達12.3°時，此時前一齒對嚙合剛結束，太陽齒與行星齒嚙合由兩齒對轉為單齒對嚙合，所以動態齒根應力出現急遽增大的現象，而在嚙合角12.3°~17.1°期間一直維持單齒嚙合狀態，所以此期間動態嚙合力都維持較大值；直到17.1°時，下一組嚙合齒對開始進入嚙合，嚙合狀態恢復為兩齒對嚙合，因此動態齒根應力快速的減小，直到27.9°整個嚙合過程結束。結果顯示動態齒根應力的變化與嚙合齒對數目改變有最直接關係，且單齒接觸時振盪次數比雙齒接觸時少但都較為劇烈。而轉速由2000 rpm提高至10000 rpm時，其動態齒根應力的變化趨勢仍顯示先由雙齒接觸開始再轉為單齒接觸最後轉回雙齒接觸直到嚙合結束；可見嚙合齒對個數還是影響動態齒根應力值的最主要因素。因為轉速的增加使得齒對嚙合時間縮短，所以振動起伏次數隨著轉速增加而減少。

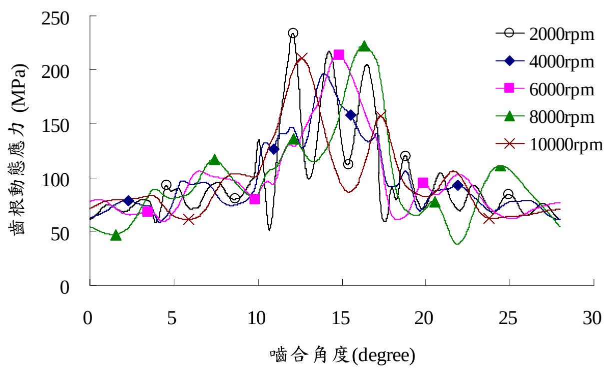

圖7扭矩150 N-m與不同轉速下，於一個嚙合週期過程中之行星齒輪動態齒根應力

5.2 連體模式結果與討論

5.2.1 連體模式穩定性

以下應用連體有限元素模式，系統阻尼比為0.075，計算行星齒輪系之動態齒根應力。圖8為輸入軸轉速在6000 rpm，扭矩為20 N-m時，行星齒輪系運轉0.0015 s ~ 0.0035 s期間共3組相鄰外齒輪對嚙合的行星齒動態齒根應力變化；結果顯示此3組嚙合齒對的動態齒根應力在趨勢和數值幾乎相同，可以看出應用本方法來分析齒輪動態響應可以達到極佳的數值穩定性。接下來以有限元素模式分析不同負載扭矩下之行星齒輪系動態，圖9為輸入軸轉速在2000

rpm分別施予20 N-m、60 N-m、150 N-m與200 N-m的扭矩時，一個嚙合週期之行星齒輪動態齒根應力變化情形；當負載扭矩呈倍數增大時，齒根動態應力的平均值約呈同比賽在增大可見本研究之所使用連體模式之行星齒輪系統動態分析方法，數值結果具有相當的正確性，而曲線之振幅大小則變化不大，進一步分析將於後面章節進行探討。

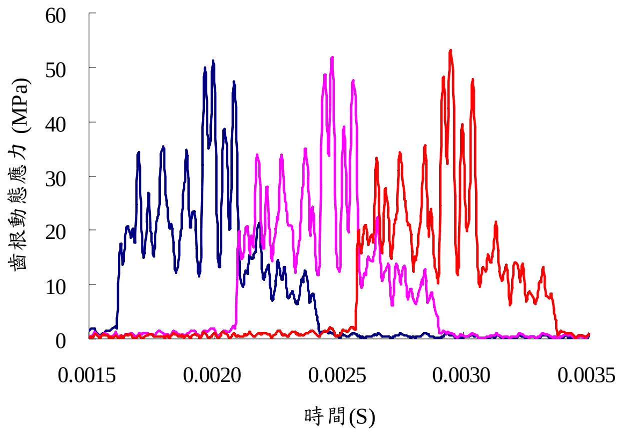

圖8 相鄰的三組外嚙合齒對中之行星齒輪動態齒根應力

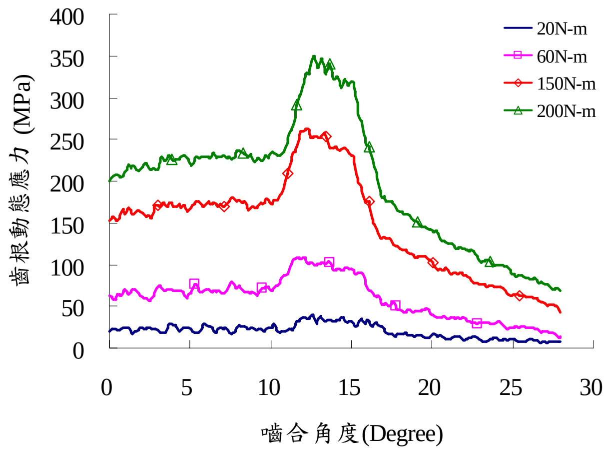

圖9 轉速2000 rpm與不同扭矩下，於一個嚙合週期過程中之行星齒輪動態齒根應力

5.2.2 連體模式動態齒根應力

接下來討論轉速與行星齒輪系動態之關係，圖10為行星齒輪系分別在輸入軸施加150 N-m的扭矩，轉速分別在2000 rpm、4000 rpm、6000 rpm、 8000 rpm與10000rpm外齒輪對之行星齒輪在一個嚙合週期過程中的動態齒根應力變化情形。圖中顯示不同轉速其動態曲線有明顯差異但是振幅大小則變化較小。曲線變化趨勢相同與離散模式的動態齒根應力有相似的趨勢，隨著轉速不斷地增加，齒對嚙合時間相對的縮短，在一個嚙合週期過程其振動次數隨之減少。

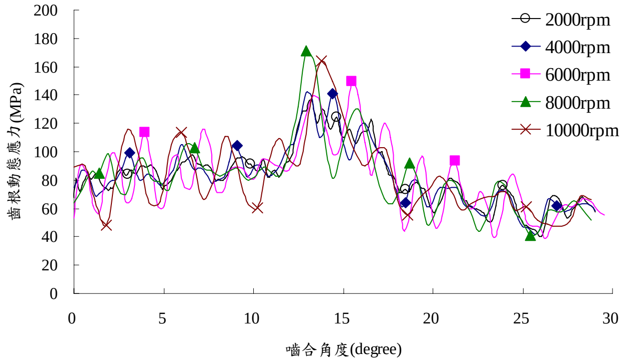

圖10扭矩150 N-m與不同轉速下，於一個嚙合週期過程中之行星齒輪動態齒根應力

5.3 離散模式與連體模式結果比較

以下分別應用離散模式與LS-DYNA之連體模式來計算行星正齒輪系之自然頻率與動態齒根應力的數值結果，兩者結果並互相比較驗證。

首先將離散模式與LS-DYNA方法的結果之自然頻率表示於圖11，結果顯示兩者之變化趨勢相同而且數值皆極為相近。可顯示兩種數值結果的正確性。

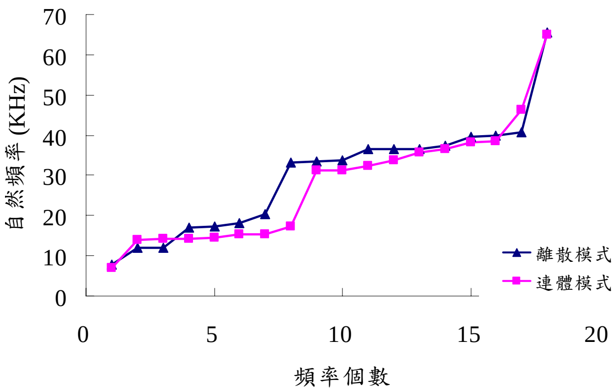

圖11 行星齒輪系之自然頻率比較

比較應用離散模式與LS-DYNA計算之動態齒根應力結果。運轉條件為輸入軸的轉數為2000 rpm，扭矩為150 N-m，而輸出軸轉數為500 rpm，系統阻尼比為0.075。圖12是離散模式與連體模式之行星齒輪的動態齒根應力比較，希望瞭解兩種方法所獲得數值結果的正確性。顯示在一個嚙合週期中，兩者所獲得之動態齒根應力變化過

程相似，行星齒輪系的外齒輪對之單齒接觸情形都發生在12.3° ~17.1° 之間，在此區間內兩種方法所獲得之動態齒根應力值都呈現較大。但結果也顯示兩種分析方法所獲得之各轉速下動態結果仍有極明顯的差異，不管在動態響應平均值與振幅大小或者動態響應曲線形狀與變化，例如以離散模式所獲得之結果均大於LS-DYNA連體模式的結果，尤其在單齒對嚙合期間的差異更為明顯，此外LS-DYNA所獲得之動態響應曲線之變化也較不規則，上述差異原因，仍待進一步分析來釐清之。

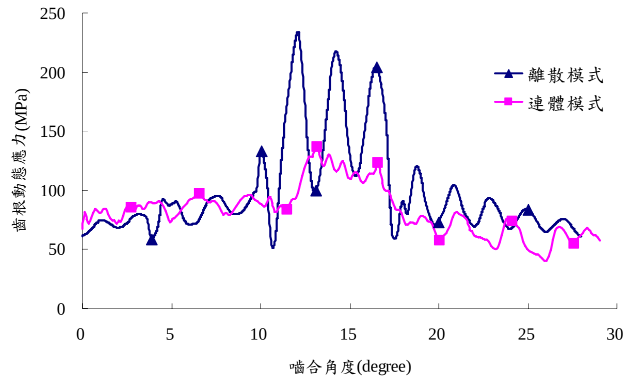

圖12 連體模式與離散模式分析動態齒根應力之比較

5.4 齒頂修整與背隙之影響

經前三小節分別探討離散模式、連體模式以及相互比較其正確性之後，本節將應用連體模式針對環齒輪之齒頂修整與齒輪背隙對行星齒輪係動態特性之影響作進一步的探討。

圖13(a)與13(b)分別表示離散模式與連體模式環齒輪齒頂高有無修整於一嚙合週期中所承受之最大齒根應力與平均齒根應力在不同轉速的比較，由此兩張圖可明顯看出當環齒輪經過修整後不管在最大或平均齒根應力的曲線趨勢都與離散模式較為一致；在環齒輪未做齒頂修整即標準齒頂高的情況下，行星齒在運轉中會與環齒輪有些微干涉，整體曲線趨勢與離散模式相反。

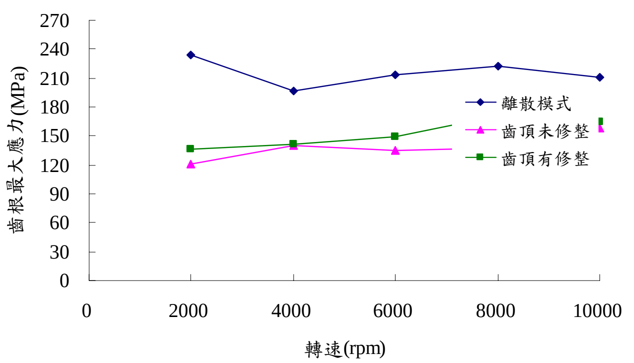

(a) 連體模式之齒頂修整與離散模式齒根最大應力比較

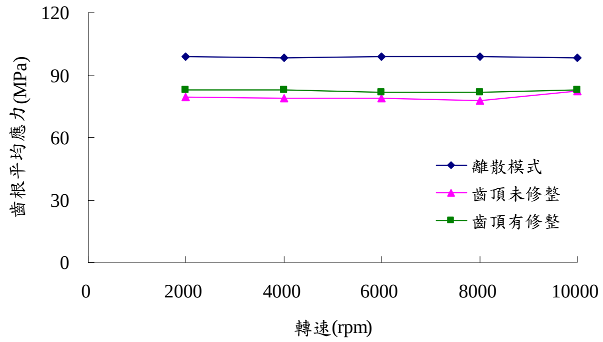

(b) 連體模式之齒頂修整與離散模式齒根平均應力比較

圖13 連體模式之齒頂修整與離散模式比較

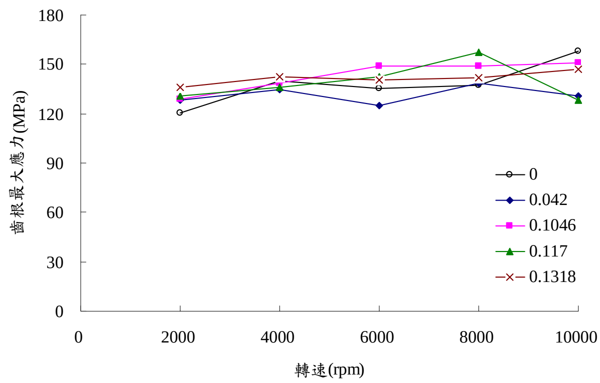

(a) 齒頂未修整不同背隙不同轉速之齒根最大應力比較

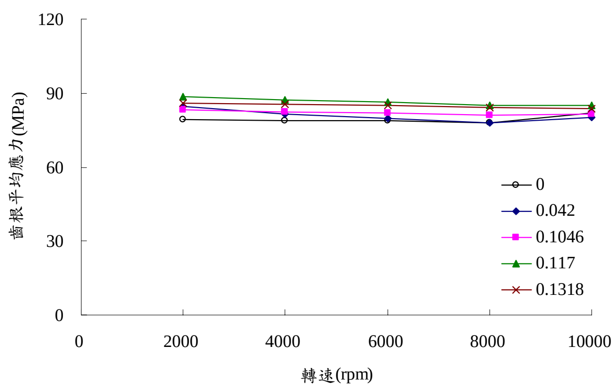

(b) 齒頂未修整不同背隙不同轉速之齒根平均應力比較

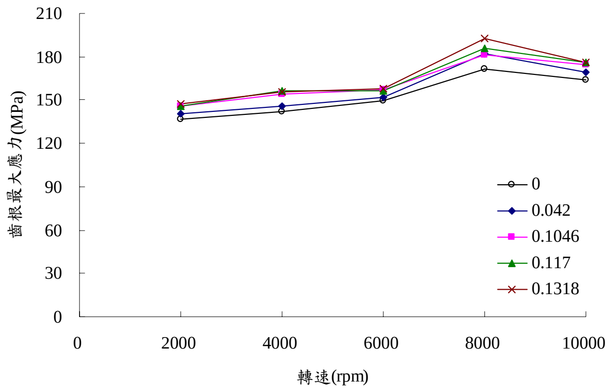

(c) 齒頂有修整不同背隙不同轉速之齒根最大應力比較

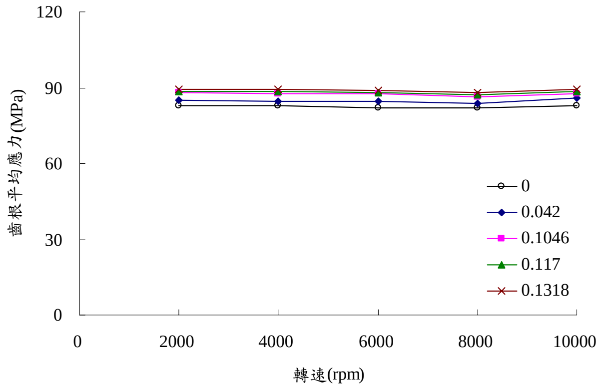

(d) 齒頂有修整不同背隙不同轉速之齒根平均應力比較

圖14 齒頂修整與背隙在不同轉速之齒根應力比較

從一系列的圖14中更能明顯看出環齒輪的齒頂是否修整對於行星齒輪系的影響。在有修整時齒根應力曲線在不同背隙值下其趨勢都是一致的，且隨著背隙量增加，所承受的齒根應力值也隨之增加；反觀齒頂未修整時，除了不同背隙之間的曲線趨勢毫無規則外，在最大背隙下所承受之齒根應力亦不是最大，由此可見環齒輪之齒頂係數之修整對於行星齒輪係是有必要性的。

在背隙對於行星齒輪系之影響的分析上我們採用理論模型即背隙值為0 mm以及0、1與2級之漸開線內、外齒輪，在0~2級齒輪最小背隙量均為0.042 mm，最大背隙量分別為0.1046 mm、0.117 mm與0.1318 mm，從圖14(d)可看出隨著背隙值由0級降至2級時其平均齒根應力值並無明顯提升，可見齒輪背隙量對於齒根應力的影響不顯著。

6. 結論

本研究已完成應用兩種行星齒輪系統時變分析之研究，分別建立了等效離散模式和LS-DYNA連體幾何模式。離散模式與連體模式結果顯示動態齒根應力的變化與嚙合齒對數目改變有最直接關係，且單齒接觸時振盪次數比雙齒接觸時少但都較為劇烈。當轉速由2000 rpm提升至 10000 rpm時，轉速的增加使得齒對嚙合時間縮短，所以振動起伏次數隨著轉速增加而減少。在相互比較之下其振動頻率與動態齒根應力在趨勢上都極為相近，可見所應用之連體模式的正確性。探討離散模式、連體模式以及相互比較其正確性後，環齒輪之齒頂修整與齒輪背隙對於行星齒輪係動態特性之影響可發現環齒輪的齒頂修整是必要的，而齒輪背隙值在理想完美外形與尺寸之行星齒輪系對於齒根應力的影響則不顯著。而影響行星齒輪系的動態之參數極多，此計畫成果可作為國內行星齒輪系統設計之參考。

參考文獻

[1] M. Botman, “Epicyclic Gear Vibration,” *ASME Journal of Engineering for Industry*, Vol. 17, pp. 811-815. (1976)

[2] A. Kahraman, “Planetary Gear Train Dynamics, ” *ASME Journal of Mechanical Design*, Vol. 116, pp. 713-720. (1994)

[3] R. B. Parker, “A Physical Explanation for the Effectiveness of Planet Phasing to Suppress Planetary Gear Vibration,” *Journal of Sound and Vibration*, Vol. 236, pp. 561-573. (2000)

[4] P. Velex and L. Famand, “Dynamic Response of Planetary Trains to Mesh Parametric Excitations,” *ASME Journal of Mechanical Design*, Vol. 118, pp. 7-14.

(1996)
[5] J. Lin and R. G. Parker, “Analytical Characterization of the Unique Properties of Planetary Gear Free Vibration,” *ASME Journal of Vibration and Acoustics*, Vol. 121, pp. 316-321. (1999)
[6] J. Lin and R. G. Parker, “Sensitivity of Planetary Gear Natural Frequencies and Vibration Modes to Model Parameters,” *Journal of Sound and Vibration*, Vol. 228, pp. 109-128. (1999)
[7] C. Yuksel and A. Kahraman, “Dynamic Tooth Loads of Planetary Gear Sets Having Tooth Profile Wear,” *Mechanism and Machine Theory*, Vol. 39, pp. 695-715. (2004)
[8] A. Bajer and L. Demkowicz, “Dynamic Contact/impact Problems, Energy Conservation, Planetary Gar Trains,” *Computer Methods in Applied Mechanics and Engineering*, Vol. 191, pp. 4159-4191. (2002)
[9] F. L. Litvin, D. Vecchiato, A. Demenego, E. Karedes, B. Hansen, and R. Handschuh, “Design of One Stage Gear Train with Improved Conditions of Load Distribution and Reduced Transmission Errors,” *ASME Journal of Mechanical Design*, Vol. 124, pp.745-751. (2002)
[10] R.G. Parker, V. Agashe, and S. M. Vijayakar, “Dynamic Response of a Planetary Gear System using a Finite Element/Contact Mechanics Model,” *ASME Journal of Mechanical Design*, Vol. 122, pp. 304-310 (2000)
[11] 梁竣傑,“行星齒輪系統動態分析,” *中華大學碩士論文*.(2006)
[12] J. H. Kuang and J. Yu, “A Dynamic Tooth Load Model of Addendum Modified Gear Pair,” *ASME Design Technical Conferences*, Vol. 71, pp. 165-176. (1994)
[13] F. L. Litvin, Gear Geometry and Applied Theory. New York.: Cambridge U. published. (2004)
[14] LSTC, “LS-DYNA Help Manual,” (2003)

計畫成果自評

本計畫已建立兩種時變模式的行星齒輪系動態分析方法，包括應用等效離散與連體幾何模式，兩者動態結果將互相比較以瞭解理論模式與數值結果的正確性。並進行了齒輪設計參數分析，討論齒輪中心距與背隙、齒頂修整、轉速與負載等條件其對於行星齒輪系動態特性之影響。本計畫已增強國內行星齒輪系統動態分析與設計之基礎。已達成達成以時變模式之行星齒輪系動態分析之計畫預期目標。研究計畫之部分成果已發表於”ASME 2207 10th International Power Transmission and Gearing Conference”。 完整成果預計發表於 97 年 3 月將投稿於國際期刊”ASME Journal of Mechanical Design”。

附件一

出席國際學術會議心得報告

計畫編號	NSC 95-2221-E-216-008
計畫名稱	以時變模式之行星齒輪系動態分析
出國人員姓名 服務機關及職稱	黃國饒（中華大學機械系副教授）
會議時間地點	96, 9/4 – 96, 9/7 , 美國 Las Vegas
會議名稱	2007 ASME International Design Engineering Technical Conferences (IDETC)
發表論文題目	Time Varying Approaches to Dynamic Analysis of a Planetary Gear System Using a Discrete and a Continuous Models

一、參加會議經過

- 9/4 下午(台灣時間) 至台灣桃園機場搭 CI-006 飛往美國 Las Vegas。
- 9/4 傍晚 (美國時間) 晚到達美國 Las Vegas。
- 9/5- 9/7 (美國時間) 全程參加 IDETC 2007，共聆聽了約 50 篇之論文發表，並提問討論。
- 9/5, 14:00-15:30 (美國時間) 進行本次發表之論文宣讀約 18 分鐘。
- 9/5, 20:00 (美國時間) 參與歡迎酒會，與各地相關研究學者討論交流。
- 9/5, 20:00 (美國時間) 參加 PTG 之晚宴，並與日本之齒輪研究學者進行討論交流。
- 9/7 晚上 (美國時間) 至 Las Vegas Mccarran 機場搭機返台。
- 9/9 早上(台灣時間) 抵台。

二、與會心得

此次為本人首次參加於國外舉辦之大型國際學術研討會，收獲極為豐碩，增加國際視野與個人研究信心。本屆 IDETC 2007 之 10th International Power Transmission and Gearing Conference (PTG)中，共有齒輪與傳動系統之研究論文共約 150 篇論文，主要包含 Design and Analysis, Dynamics and Noise, Strength and Durability 之領域論文為最多。本人此次發表之論文為提出關於行星齒輪系統之動態分析方法，將可以應用於廣泛行星齒輪系統之動態研究與設計應用，口頭報告結束後並與現場提問者交流討論。此外全程參與研討會各分組之論文發表，共聆聽

了約 50 篇之論文發表，主要為 Design and Analysis, Dynamics and Noise, Strength and Durability, manufacturing 相關研究為主，並與論文發表者進行交談，討論到關於如螺旋齒輪對應力分析、齒輪摩擦力量測、齒輪潤滑實驗、非線性動態模式、行星齒輪系統之非線性動態模式與響應等課題。會議中場休息以及用餐時間，本人也盡量主動與各國與會學者交談，進行廣泛交流。在此次首次參加國外之大型國際研討會，雖然在美時間只有三天，收穫感觸皆多。

個人認為，在未來齒輪系統之發展仍有無限發展的可能，包括更高轉速，更精密的傳動，更長的壽命以及更可靠的運轉。隨著當今環境保護與永續能源之發展，中華大學位於新竹應有所投注，尤其關於**大型風力發電系統用齒輪系統之發展**，包括更大發電容量、振動噪音防治、可靠度、系統整合之研究，建議隨著能源與環保之議題之趨勢，臺灣之產業發展彰顯特色與永續經營考慮時，此領域是特別值得注意投入的。。

Proceedings of the ASME 2007 International Design Engineering Technical Conferences & Computers and Information in Engineering Conference
IDETC/CIE 2007
September 4-7, 2007, Las Vegas, Nevada, USA

附件二

DETC2007/ 34100

TIME VARYING APPROACHES TO DYNAMIC ANALYSIS OF A PLANETARY GEAR SYSTEM USING A DISCRETE AND A CONTINUOUS MODELS

K. J. Huang *
Department of Mechanical Engineering

C. C. Liang
Department of Mechanical Engineering

J. Y. Chen
Department of Mechanical Engineering
Chung Hua University,
No. 707, Sec. 2, Wu Fu Rd, Hsin Chu, Taiwan (30067), R.O.C..

ABSTRACT

Two time varying approaches are executed in analyzing dynamics for an involute planetary gear system, which respectively use a conventional discrete model of the equivalent mass-damping-spring elements and a continuous geometry model by the finite element method. In the discrete approach, the tooth number, position, and phasing difference of the meshing tooth pairs are described by time varying and nonlinear meshing stiffnesses. Natural frequencies, deformations, meshing forces, fillet stresses, and dynamic factors can be calculated by using the Jacobi transformation and the Runge-Kutta integration. In the continuum approach, dynamics of the planetary gear system is analyzed using the software, LS-DYNA. The approach of the continuous geometry model can incorporate the time varying properties intrinsically. In this continuum study, not CAD models, high quality mesh elements of the planetary gear system are automatically generated directly using the derived tooth profile equations. After assigning initial and boundary conditions, dynamic responses for the planetary gear system are solved. Natural frequencies and fillet stresses of the both approaches are verified by each other comparison. Potentially, the continuum approach can extensively and sophistically analyze dynamics problems of the planetary gear systems.

1 INTRODUCTION

Constantly, the gearing is the most important transmission solution in the majority of machineries. Among that, due to their excellent features of high precision, high reduction ratio, high power-volume ratio, and low noise and vibration, planetary gear sets have been applied in the wide varieties of high technology machinery such as vehicles, aircrafts, machine tools, and robots et al. With increasingly severe demands for high precision and high speed transmission mechanisms, dynamic performance of gearings has to be further upgraded. Thus inclusion of planetary types, dynamic analysis of gearings has become the important research topic.

Three decades ago, the researcher [1] has originally performed the dynamic investigation of planetary gear systems. Latter, August and Kasuba [2] found that dynamic responses of planetary gear systems are critically affected by the variation of the meshing stiffnesses and fixity design of their sun gears and stated that a design using a stationary sun gear has better dynamic performance than a floating one. In 1996, Velex and Flamand [3] also obtained the similar conclusion. Of high creativity, Kahraman [4] investigated the dynamics of a helical planetary gear system with four equally spacing planet gears. The author categorized planet phasing conditions and also calculated modal shapes and meshing forces caused by the excitation due to profile errors in the gear system. Not long ago, Parker [5, 6] also investigated influence of the meshing phase differences on the dynamics for the planetary gear systems designed with three and four planet gears. Besides, the publication of Velex and Flamand [7] presented that the stiffnesses of the meshing gear pairs influence the planetary gear dynamics than the stiffnesses of the shafts, sun and ring gears, and bearings do. Recently, the effect of nonlinearity in the planetary gearings also started to be emphasized. Sun and Hu [8] using a harmonic balance method analyzed the nonlinear dynamics of planetary gearings both incorporating the nonlinearity of multiple clearances and time varying meshing stiffnesses. Lin and Parker [9] calculated natural frequencies of planetary gear systems. The nonlinearity due to meshing stiffness discontinuity of gear pairs was discussed. Moreover, the same authors [10] also discussed the natural frequencies and their repetition number of the planetary gearings in which the vibration modes are classified into three types of the rotational, translational, and planetary modes.

* Associate Professor and author of correspondence, Phone: Tel: (886) 35186743, Fax: (886) 35186521, Email:kjhuang@chu.edu.tw

Virtually, difficulties of dynamic analyses for planetary gear systems are caused by their diversity and complexity of system configuration, numerous design parameters, required precise description of their complicated tooth profiles, and many others. A conventional equivalent discrete model can greatly simplify their physical model and benefit computing efficiency. However, not only the complexities of structure configuration and geometry profiles, but also the time varying and nonlinear behaviors of meshing stiffness due to move contact points and number of tooth pairs in contact, meshing stiffness discontinuity, and backlash; the discrete model is hard to describe the planetary gearings precisely. Needless to say, the considerations of the profile modification, manufacturing error, elastic deformation, and lubrication and wear are never too emphasized in the gear design. Probably, it may be stated that using the discrete model is only adequate to limitative types of planetary gearing under very simplified designs and operating considerations.

With improvement of computer and computing technologies, analyzing methods employing the 2D/3D continuum models are becoming mature and have been successfully applied in lots of engineering applications. The methods being applied in the gear dynamic analyses are naturally considered, through that more complicated problems and accurate results about gear dynamics are expected to be arrived. Thus, Huang and Liu [11] utilized a dynamic stiffness method of a continuous geometry model in which each gear tooth is described using four nonuniform Timoshenko beam elements. Through that, dynamic response of spur gear pairs including the effect of tooth modifications and backlashes was investigated. Tsai and Tsai [12] and Litvin et al. [13] performed the statics analysis of a gear using the FEM method. Recently, Chen and Tsay [14] also used the commercialized package, ABAQUS, to analyze static contact forces in the helical gear pairs. When analyzing gear statics or dynamics problems by the continuous approaches, high quality element models, which precisely describe the gear geometric profiles, have to be prepared in advance. However, there exist difficulties owing that (i) the tooth profile is constituted by complex curves, (ii) large dimension aspect ratio exists between a whole gear and its critical areas such as the points near a local contact and tooth fillet, and (iii) once the influences of tooth profile modification, manufacturing error, and backlash are concerned. Even for a simplest gear pair, the preparation of its element model is a very time-consuming and high skilled burden. Therefore, Brauer [15] using the gear geometry theory of Litvin [16] presented a method to generate element models applicable to several gear types automatically.

In the aspect of planetary gear systems, Yuksel and Kahraman [17] used an FEM package to calculate the dynamic meshing forces and predicted their wear on gear teeth. The influence of wear on the dynamic response for the planetary gear systems is also discussed. The authors concluded that severe wear causes an obvious effect on the vibration modes and also on the dynamic meshing forces for the gearing. Besides, using the multibody model and the contact theorem, Bajer and Demkowicz [18] analyzed the dynamic responses of a planetary gearing subjected to an impact. The total system energy including both the effects of the rigid and elastic is calculated. Recently, Litvin et al. [19] undertook a tooth contact analysis by performing tooth profile and crowning modifications through which the transmission error, noise and vibration of a planetary gearing were expected to be reduced. Basically, the above gear studies using continua are mainly endeavored on static mechanics. Until the recent studies [17, 20], the continuum approach using the finite element method is starting to be adopted in analyzing gear dynamics.

This study proposes two generalized time varying approaches to dynamic analysis of an involute planetary gear system, which are respectively using a conventional discrete model and a continuous geometry one. In the discrete approach, time varying meshing stiffnesses of sun-planet and ring-plant tooth pairs will be derived. Through that, the number, position, phasing difference of meshing tooth pairs are included. In the continuous geometry approach, the element models of high quality for the planetary gear system are automatically generated directly using the derived tooth profile equations. Then, dynamic responses of the planetary gear system are solved both using the dynamic FEM software of general purpose, LS-DYNA.

2 DISCRETE APPROACH

2.1 Equations of Motion

Figure 1(a) shows a 3D solid model of a planetary spur gear system. The fixed ring gear is ground to the stationary frame. The torque applying on the shaft of the sun gear is transferred to the output shaft which is connecting to the carrier. The equivalent 2D discrete model of the gear system is depicted in Fig. 1(b). Here, the Lagrange equation will be served to derive the equation of motion for the planetary gear system. Firstly, the assumptions for the theoretic derivation are given as follows: (1) the planetary gear system is described by a 2D discrete model, (2) the meshing stiffness of a mating gear pair is modeled by connecting tangentially their base circles using a translational spring, (3) all bearings are modeled using supporting translational springs, (4) no manufacturing errors exist, and (5) neglect the effect of deformation of the carrier on planet gears. Besides, in order to brief the description, an external gear pair means a gear pair of the sun and a planet gears, and an internal gear pair for a gear pair of a planet and the ring gears. Then including the rigid body rotation, the kinetic and strain energies in the planetary gear system are derived in Eqs. (1) to (13).

Kinetic energy:

$$T^{(d)} = \frac{1}{2} J^{(d)} \left(n^{(d)} + \dot{\phi}^{(d)}\right)^2 \tag{1}$$

$$T^{(s)} = \frac{1}{2} J^{(s)} \left(n^{(s)} + \dot{\phi}^{(s)}\right)^2 + \frac{1}{2} m^{(s)} \left[\left(\dot{x}^{(s)}\right)^2 + \left(\dot{y}^{(s)}\right)^2\right] \tag{2}$$

$$\begin{aligned} T^{(i)} &= \sum_{i}^{n_P} \frac{1}{2} J^{(i)} \left(n^{(i)} + \dot{\phi}^{(i)}\right)^2 \\ &\quad + \sum_{i}^{n_P} \frac{1}{2} m^{(i)} \left[\left(-r_b^{(c)} n^{(c)} \sin \Psi_i + \dot{x}^{(i)}\right)^2 \right. \\ &\quad \left. + \left(r_b^{(c)} n^{(c)} \cos \Psi_i + \dot{y}^{(i)}\right)^2\right] \end{aligned} \tag{3}$$

$$T^{(c)} = \frac{1}{2} J^{(c)} \left(n^{(c)} + \dot{\phi}^{(c)}\right)^2 \tag{4}$$

$$T^{(r)} = \frac{1}{2} J^{(r)} \left(n^{(r)} + \dot{\phi}^{(r)}\right)^2 + \frac{1}{2} m^{(r)} \left[\left(\dot{x}^{(r)}\right)^2 + \left(\dot{y}^{(r)}\right)^2\right] \tag{5}$$

$$T^{(o)} = \frac{1}{2} J^{(o)} \left(n^{(o)} + \dot{\phi}^{(o)}\right)^2 \quad (6)$$

Strain energy：

$$V^{(ds)} = \frac{1}{2} k^{(ds)} \left(\phi^{(d)} - \phi^{(s)}\right)^2 \quad (7)$$

$$V^{(s)} = \frac{1}{2} k^{(sx)} \left(x^{(s)}\right)^2 + \frac{1}{2} k^{(sy)} \left(y^{(s)}\right)^2 \quad (8)$$

$$V^{(si)} = \frac{1}{2} k^{(si)} \left(d^{(si)} - E^{(si)}\right)^2, i = 1,..,n_P \quad (9)$$

$$V^{(ri)} = \frac{1}{2} k^{(ri)} \left(d^{(ri)} - E^{(ri)}\right)^2 \quad (10)$$

$$\begin{aligned} V^{(c)} &= \sum_{i}^{n_P} \frac{1}{2} k^{(cix)} \left(x^{(i)} + r_b^{(c)} \phi^{(c)} \sin \Psi_i\right)^2 \\ &+ \sum_{i}^{n_P} \frac{1}{2} k^{(ciy)} \left(y^{(i)} - r_b^{(c)} \phi^{(c)} \cos \Psi_i\right)^2 \end{aligned} \quad (11)$$

$$V^{(r)} = \frac{1}{2} k^{(rx)} \left(x^{(r)}\right)^2 + \frac{1}{2} k^{(ry)} \left(y^{(r)}\right)^2 \quad (12)$$

$$V^{(oc)} = \frac{1}{2} k^{(oc)} \left(\phi^{(o)} - \phi^{(c)}\right)^2 \quad (13)$$

where $T^{(*)}$ and $V^{(*)}$ are the kinetic and strain energies, respectively; $J^{(*)}$ the polar inertial moments; $m^{(*)}$ and $k^{(*)}$ the masses and stiffnesses, respectively; $n^{(*)}$ and $\dot{\phi}^{(*)}$ the rigid and elastic rotation speeds, respectively; and $\dot{x}^{(*)}$ and $\dot{y}^{(*)}$ the translational velocities of elastic deformations, respectively. The superscript * can be *d*, *s*, *c*, *i*, *r*, and *o* which respectively represent the input shaft, sun gear, carrier, *i*th planet gear, ring gear, and output shaft. More explanation, $V^{(d)}$ is the strain energy of the driving shaft, $V^{(s)}$ strain energy of the sun gear, $V^{(si)}$ strain energy between the sun gear and the *i*th planet gear, $V^{(ri)}$ strain energy between the ring gear and the *i*th planet gear, $V^{(ci)}$ strain energy between the carrier gear and the *i*th planet gear, $V^{(r)}$ translational strain energy of the ring gear, and $V^{(oc)}$ strain energy of the driven gear. Besides, $r_b^{(*)}$ and $r_a^{(*)}$ represent the radii of the base and addendum circles of the gears, respectively, and n_P is the number of the planet gears. Besides, $d^{(si)}$ in Eq. (9) and $d^{(ri)}$ in Eq. (10) are the elastic deformations along the contact lines between the *i*th planet gear to the sun gear and to the ring gear, respectively. $E^{(si)}$ and $E^{(ri)}$ are the errors of the sun and the ring gears, respectively. As the illustration in Fig. 2, $d^{(si)}$ and $d^{(ri)}$ can be formulated as

$$\begin{aligned} d^{(si)} &= \left(r_b^{(s)} \phi^{(s)} + x^{(s)} \cos \eta_i + y^{(s)} \sin \eta_i\right) \\ &- \left(r^{(i)} \phi^{(i)} + x^{(i)} \cos \eta_i + y^{(i)} \sin \eta_i\right) \end{aligned} \quad (14)$$

$$\begin{aligned} d^{(ri)} &= \left[r_b^{(r)} \phi^{(r)} + x^{(r)} \sin\left(\alpha_{rp} + \Psi_i\right) + y^{(r)} \cos\left(\alpha_{rp} + \Psi_i\right)\right] \\ &- \left[r_b^{(p)} \phi^{(i)}{}_{pi} + x^{(i)}{}_{pi} \sin\left(\alpha_{rp} + \Psi_i\right) + y^{(i)} \cos\left(\alpha_{rp} + \Psi_i\right)\right] \end{aligned} \quad (15)$$

where α_{sp} and α_{rp} are the operating pressure angle of the external and the internal gear pairs, respectively. Then, using the Lagrange equation to Eqs. (1)-(13) and including damping terms, the discrete governing equation for vibration of the planetary gear system expressed in a matrix form is derived and expressed as

$$\mathbf{M}\ddot{\mathbf{x}} + \mathbf{C}\dot{\mathbf{x}} + \mathbf{K}\mathbf{x} = \mathbf{F} \quad (16)$$

where $\mathbf{M}$, $\mathbf{C}$, and $\mathbf{K}$ are the matrices of mass, damping, and stiffness respectively. $\mathbf{x}$ and $\mathbf{F}$ are the displacement and the excitation vectors, respectively. The deriving process and the elements in the matrices and vectors in Eq. (16) are abundantly given in Ref. [21]. Subsequently, meshing stiffnesses and phase differences, which can simulate the time varying properties of the planet gear system, are deduced as follows.

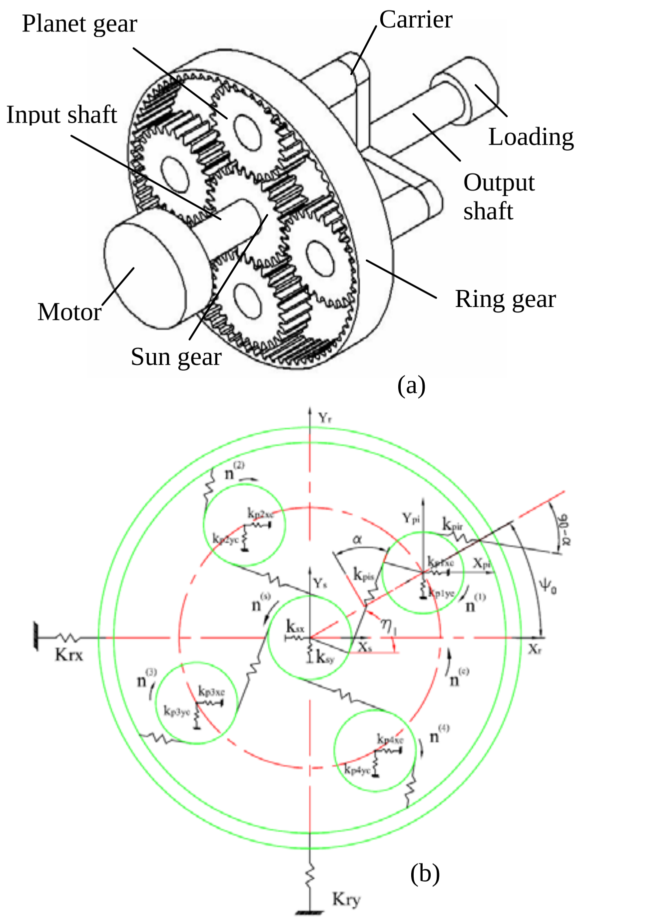

Figure 1. A planetary spur gear system: (a) 3D solid model, (b) 2D discrete physical model.

2.2 Meshing Stiffnesses of Gear Pairs

In this study, using the method proposed by Kuang and Lin [22], the meshing stiffnesses of the gear pairs in the planetary gear system can be obtained by including three parts of compliance: (i) q_{Tj} due to gear tooth subject to the meshing forces, (ii) q_{Bj} due to the elastic support of the gear body, and (iii) q_{Hj} due to the local deformation by the Hertz contact stress. Therefore, the meshing stiffness $k_{pg,j}$ for the *j*th tooth pair in the mating gears, *p* and *g*, can be expressed as

$$k_{pg,j} = (q_{Tj} + q_{Bj} + q_{Hj})^{-1} \quad (17)$$

Including all tooth pairs engaging the mesh at the instant, their resulting stiffness for the gear pair is obtained as

$$k_{pg}=\sum_{j=1}^{n_T} k_{pg,j} \tag{18}$$

where n_T is the number of the meshing tooth pairs.

2.3 Phase Differences between Gear Pairs

In a similar way to Ref. [6], the phase differences are derived. Figures 2 and 3 illustrate the meshing conditions of various external and internal gear pairs. Respectively, C_i and $\mathrm{C}_i^{'}$ are the meshing points of the external and internal gear pairs and P_i and $\mathrm{P}_i^{'}$ are their operating pitch points. $r_a^{(*)}$ and $r_b^{(*)}$ are the radii of addendum and base circles in which superscripts * can be *s*, *p*, and *r* which respectively represent the sun, planet, and ring gears. r_{C_i} and $r_{C_i^{'}}$ are the radii at the contact points and $z^{(s)}$ and $z^{(r)}$ the teeth numbers of the sun and ring gears. In addition, the share angles for each gear tooth are $2\pi / z^{(s)}$ and $2\pi / z^{(r)}$ which are respectively for the sun and ring gears. $\psi_c^{(k)}$ is the circumferential angle between the *k*th and first planet gears around the sun gear. Abundantly, two kinds of phase differences between the individual meshing gear pairs are respectively derived below.

(1) Phase difference between *k*th and 1st external gear pairs

Firstly, assume that the first external gear pair is meshing at the pitch point P_1 as shown in Fig. 2. Then, the passing teeth number, counting from the first planet gear to the *k*th one around the sun gear, can be calculated using Eq. (19).

$$\frac{\psi_c^{(k)}}{2\pi / z^{(s)}} \quad \text{or} \quad \frac{\psi_c^{(k)} \cdot z^{(s)}}{2\pi} \tag{19}$$

There are two conditions discussed as follows:

(a) The result of Eq. (19) is an integer, i.e.,

$$\frac{\psi_c^{(k)} \cdot z^{(s)}}{2\pi}=\operatorname{int}\left(\frac{\psi_c^{(k)} \cdot z^{(s)}}{2\pi}\right) \tag{20}$$

which means that no phase difference exists between these two gear pairs. Here, int is defined as an operator to acquire the integral part.

(b) The result of Eq. (19) is not an integer. The passing number of the sharing angles for each tooth around the sun gear from the first planet gear to the *k*th one is

$$n^{(s)}=\operatorname{int}\left(\frac{\psi_c^{(k)} \cdot z^{(s)}}{2\pi}+1\right) \tag{21}$$

Thus, the phase difference exists between the *k*th and the first gear pairs and is derived as follows. Using the illustration in Fig. 2, the angle between the radial line of the starting point of involute for the sun gear in the *k*th gear pair and center line $\overline{O_k O_s}$ is given as

$$\theta_1=\frac{2\pi \cdot n^{(s)}}{z^{(s)}}-\psi_c^{(k)}+\operatorname{inv}\alpha_{sp} \tag{22}$$

where inv is the involute function [14]. Thus, the phase difference, $\kappa_{sp}^{(k)}$, between the *k*th and the first external gear pairs can be as follows:

(i) when $r_{C_k} \geq r_a^{(s)}$, $\kappa_{sp}^{(k)}=\theta_1-\frac{2\pi}{z^{(s)}}-\operatorname{inv}\alpha_{sp}$.

(ii) when $r_{C_k} < r_a^{(s)}$, $\kappa_{sp}^{(k)}=\theta_1-\operatorname{inv}\alpha_{sp}$.

If $\kappa_{sp}^{(k)}>0$, the *k*th external gear pair is leading to the first one with a phase angle of $\kappa_{sp}^{(k)}$. Oppositely, if $\kappa_{sp}^{(k)}<0$, the *k*th external gear pair is phase lagging to the first one with an angle of $-\kappa_{sp}^{(k)}$.

In a similar derivation using Fig. 2, the phase difference between the *k*th and the first internal gear pairs can also be derived but no detail is shown here.

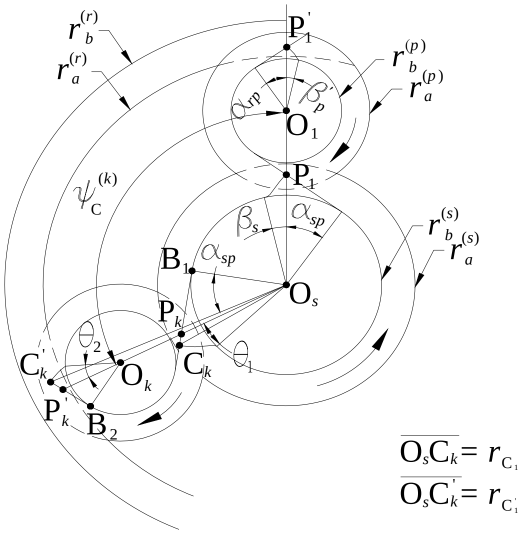

Figure 2. Meshing phasing relation between the *k*th and the 1st gear pairs of the external and the internal.

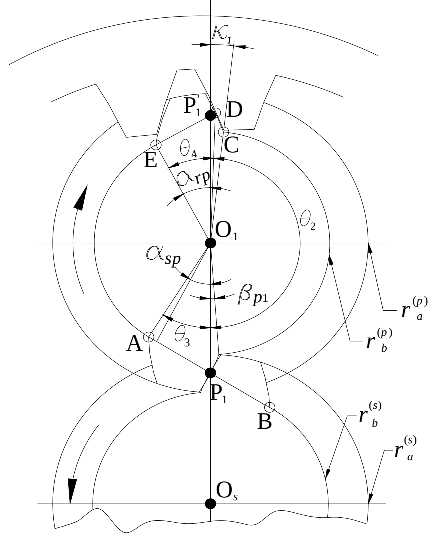

Figure 3. Meshing phase relation between the 1st external and the internal gear pairs.

(2) Phase difference between the 1st external and internal gear pairs

The phase relation between the first external and the first internal gear pairs is derived from the configuration illustrated in Fig. 3. Again, assume that the first external gear pair is meshing at the pitch point, P_1. Designate κ_{sr} to be the phase difference between the first internal gear pair and the first external one. As the illustration in Fig. 3, the angle between the radial line at the involute starting point of the planet gear in the first internal gear pair and the center line $\overline{O_1O_s}$ is

$$\beta_{p1} = \text{inv}\alpha_{sp} \tag{23}$$

Thus, the angle θ_3 between the radial line of the starting point, A, of the opposite involute curve of the planet to center line $\overline{O_1O_s}$ is

$$\theta_3 = \frac{t_p}{r_b^{(p)}} + 2\text{inv}\alpha_0 - \beta_{p1} \tag{24}$$

where α_0 is the pressure angle of the rack cutter and t_p, which is the circular tooth thickness at the pitch circle, is written as

$$t_p = \pi m/2 + 2e\tan\alpha_0 \tag{25}$$

Here, m is the module of the gear and e is the amount for the nonstandard tool setting. Combining Eqs. (23) to (25) leads to

$$\theta_3 = \frac{\pi}{z^{(s)}} + \frac{2e\tan\alpha_0}{mz^{(s)}} + 2\text{inv}\alpha_0 - \text{inv}\alpha_{sp} \tag{26}$$

Next, by passing teeth number counting around the planet gear along its rotation direction, find out its first tooth, which has exceeded center line $\overline{O_1O_s}$ and is joining the meshing of the internal gear pair. Then, the passing teeth number n_1 can be found using Eq. (27).

$$\frac{\pi - \theta_3}{2\pi / z^{(p)}} \tag{27}$$

(a) If Eq. (27) is an integer, then

$$n_1 = (\pi - \theta_3)/(2\pi / z^{(p)})$$

(b) If Eq. (27) is not an integer, then

$$n_1 = \text{int}[(\pi - \theta_3)/(2\pi / z^{(p)}) + 1]$$

Therefore, the angle κ_1 between the radial line of the involute starting point, C, on the first planet gear and center line $\overline{O_1O_s}$ is

$$\kappa_1 = n_1 \cdot \frac{2\pi}{z^{(p)}} + \theta_3 - \pi \tag{28}$$

Using relation $\overline{ED} = \widehat{EC}$ can lead to

$$\theta_4 = \tan^{-1}(\alpha_{rp} + \kappa_1) \tag{29}$$

Finally, the phase difference between the first internal to the first external gear pairs is

$$\kappa_{sr} = \text{inv}\theta_4 - \text{inv}\alpha_{rp} \tag{30}$$

If $\kappa_{sr} > 0$, the first internal gear pair is leading to the first external one with a phase angle of κ_{sr}. If $\kappa_{sr} < 0$, then the first internal gear pair is lagging to the first external one with a phase angle of $-\kappa_{sr}$. Using the above derivations, the meshing phase differences for the planetary gearing between the arbitrary two gear pairs can be obtained.

2.4 Dynamics Analysis by Discrete Approach

Subsequently using the model derived above, the dynamic analysis to the planetary gear system using the discrete approach can be achieved. Firstly, the instantaneous meshing points, the number of tooth pairs in contact, and the phase differences, the corresponding instantaneous and equivalent meshing stiffnesses of the gear pairs are calculated. Then, the time varying governing equations for dynamic analysis to the planetary gear system are obtained. Next, executing the Jacobi transformation, the natural frequencies of the planetary gear system are found. Finally, applying the driving and the driven torques on the shafts, updating the time varying elements, and performing the Runge-Kutta integration, the dynamic displacements of the gearing are obtained. Thus, its fillet stresses, dynamic meshing forces, and dynamic factors in the gearing can also be calculated. The dynamic factor here is defined as the ratio maximum between the dynamic meshing forces to the static ones in the planetary system.

3 CONTINUOUS APPROACH

3.1 FEM Model of Planetary Gear System

The planetary gear system investigated is constituted by standardized involute spur gears. Its mesh element model is created through the following process. Firstly, by using the homogenous coordinate transformation on the profile equations of a rack cutter and applying the equation of meshing for gears, the theoretic tooth profiles of the gears are obtained. Then, not CAD models but using a C code, high quality meshing elements of the gears are automatically built by using the derived tooth profile equations directly. By which, the mesh elements of the sun gear, planet gears, and ring gear are sequentially created. Next, including the models of the driving and driven shafts, carrier, bearings, and bearing house, the entire model of the planetary gear systems is built as shown in Fig.4. Then, after assigning suitable material properties, initial and boundary conditions, and other required settings, dynamic responses for the planetary gear system can be solved. Figure 4 shows the FEM model of the analyzed gear system whose gear data are given as follows: module $m = 1.25$ mm, pressure angle $\alpha_0 = 20^0$, tooth number $z^{(s)} = z^{(p)} = 28$, $z^{(r)} = 84$. The bearing houses are used to accommodate the bearings, whose effect is modeled by using discrete supporting springs herein.

3.2 LS-DYNA Settings for Gear Dynamics

Assign the material and element properties to the created element model of components in the planetary gear system. A specified steel type is assigned material to all the components. The carrier is assumed with high rigidity for its minor deformation. Additionally, the elastic displacements of the input and the output shafts, bearing houses, and carrier are neglected. Thus, their rigid body property is also assumed. Next, contact conditions between the meshing gear pairs will be defined. Define that the driving ones are masters and the driven ones are slaves. Thus for an external gear pair, the sun gear is a master and the planet gear is a slave. For an internal gear pair, the planet gear is a master and the ring gear is a slave. The input shaft is rigidly connected to the sun gear using constraint "Extra Node" [23], so is the output shaft connected to the carrier. Then, boundary conditions of a constant driving torque applied on the input shaft, and a prescribed constant rotation speed is given to the output shaft those are depicted in Tab. 1. The settings corresponding to numerical computing and output control are also given. Finally, the dynamic responses of the planetary gearing by the continuous approach are calculated using LS-DYNA.

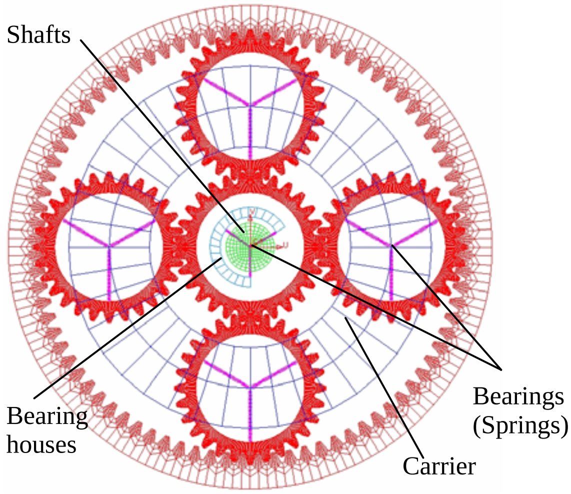

Figure 4. The mesh element model of the planetary gear system.

Table 1. Settings of boundary and initial conditions for analyzing the planetary gear system using LS-DYNA.

Shaft	Setting
Input shaft	1. Constraint: rigidly connecting input shaft and sun gear using "Extra Node" 2. Initial condition: initial rotation speed 3. Driving torque
Output shaft	1. Constraint: rigidly connecting output shaft and carrier using "Extra Node" . 2. Initial condition: initial rotation speed 3. Prescribed motion

4 RESULTS AND DISCUSSION

4.1 Equivalent Meshing Stiffness

Although the proposed models can deal with general planetary gear systems, only the one with four equally spacing planet gears is an example here. Firstly, the equivalent meshing stiffnesses of the analyzed external and internal gear pairs during a meshing cycle are calculated. The meshing stiffness, shown in Fig. 5, at instant of mesh beginning for the external gear pair is 3.63×10^8 N/m. At this instant, the number of tooth pairs in contact is double. When the meshing angle is arriving at 4.7°, the meshing stiffness achieves to a maximum value of 3.87×10^8 N/m. When the angle to the instant of 8.2°, the tooth pair in contact is single since the leading tooth pair ends its meshing. Then, at instant 12.9° tooth pairs in contact return to double again. Eventually, to the angle of 21.1°, the meshing cycle of the tooth pair is completed. The maximum stiffness of 3.87×10^8 N/m appears twice at the instants of 4.7° and 17.6°, respectively. However, the maximum for the interval of single tooth pair in contact only is 2.19×10^8 N/m that occurs at 10.8° at which the mating teeth are contacting near their pitch points. The stiffness of the external gear pair is symmetric to the middle instant of meshing at the pitch points. Besides, assume that the stiffness of the internal gear pair in Fig. 5 is one and half a times of the value of the external one. The two curves exhibit the phase difference between the external and the internal gear pairs in the planetary gear system.

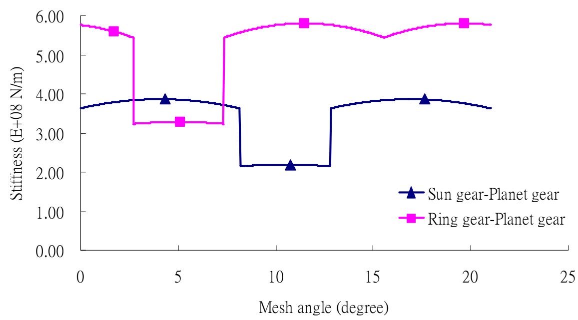

Figure 5. Meshing stiffnesses of external and internal gear pairs during a meshing cycle.

4.2 Dynamic Meshing Force

Figure 6 shows the dynamic meshing forces in the external and internal gear pairs during one meshing cycle when the rotation speed of the sun gear is 2000 rpm. Firstly, the meshing forces between the sun gear and the first and third planet gears in the external gear pairs shown are discussed. As shown in Fig. 6(a), at the beginning of this meshing period, the number of tooth pairs in contact is two. At this instant, the meshing force is 131 N. With the progress of the rotation angle, the meshing force is increased. Then, to the instant of 12.3°, the leading tooth pair ends its meshing cycle, the condition of tooth pairs in contact change from double to single. Thus, the meshing force is suddenly increased. The condition of the engaging tooth pair is single during the interval, 12.3° to 17.1°. Therefore, at which, the force maintains a larger value. Until to the instant after 17.1°, the next tooth pair starts its meshing process. The condition reverses to the double tooth pairs in mesh again. Thus, the force becomes evidently small during this interval. Finally, decreasing tendency is maintained to the end of meshing for the tooth pair.

The result shows that the dynamic meshing force is essentially affected by the number of tooth pairs in contact. Besides, the meshing forces of the first and the third external gear pairs are exactly same, which also exhibit axially symmetric to the sun gear. Also, the forces of the second and the fourth pairs are same. Noticeably, the meshing forces between the neighbor planet gears, e.g. the first and the second ones, have a little of difference. Whereas, the changing tendency of the all meshing forces shows totally same since no phase differences exist among these four external gear pairs. Besides, the meshing forces between the planet and the ring gears for the internal gear pairs are shown in Fig. 6(b). Although, the dynamic meshing forces of the external and the internal gears are very close, however, their changing tendencies are quite different because that there exists the phase difference between the external and the internal gear pairs.

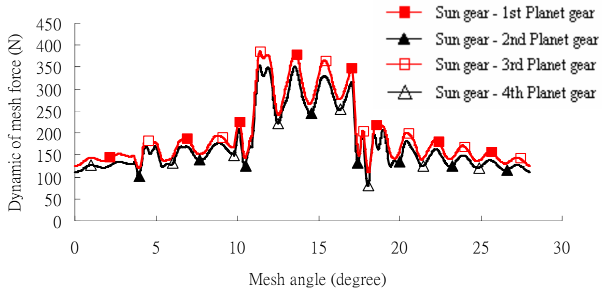

(a)

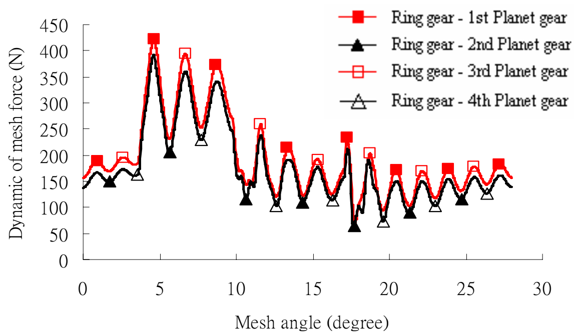

(b)

Figure 6. Dynamic meshing forces of the planetary gear system during a meshing cycle of tooth pairs: (a) in the external gear pairs, (b) in the internal gear pairs.

4.3 Results Comparison

Using LS-DYNA, this section calculates the dynamic responses of the planetary gear system using the continuous approach. Natural frequencies and dynamic fillet stresses calculated from the continuous model will compare with the results from the discrete one.

Firstly, the natural frequencies obtained by the discrete and the continuous methods are shown in Fig. 7. The agreement of the both results basically exhibits correctness of the both approaches. Next, the numerical dynamic fillet stresses of the both approaches are displayed. The input shaft is assigned a constant speed of 2000 rpm and a driving torque of 20 N-m. Thus, the rotation speed of the output shaft is 500 rpm. The assigned system damping ratio is 0.075. Figures 8 compare the dynamic fillet stresses in the sun gear for the external gear pair and that in the planet gear for the internal gear pair, respectively. The dynamic results from the both methods are close in amplitude and in tendency. This comparison verifies the numerical correctness of the proposed approaches but only roughly because indispensable deviation still exists between them. Currently, further investigations are being undertaken by the authors. Finally, by using the discrete approach in the time varying model, the dynamic factor of meshing force for the external gear pair is calculated. Figure 9 shows the dynamic factor of an external gear pair. Expectedly, both the discrete and continuous approaches presented here can investigate dynamic responses of the planetary gear system extensively and completely.

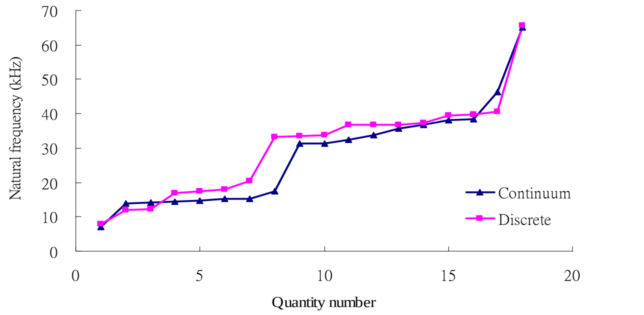

Figure 7. Comparison of natural frequencies of the planetary gear system calculated by the discrete and continuous models.

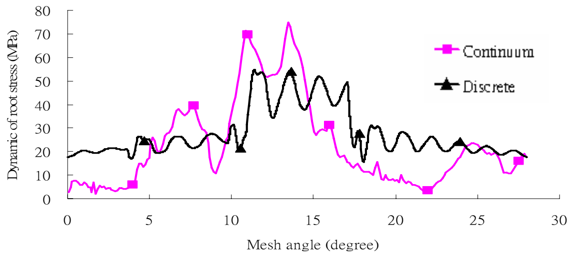

(a)

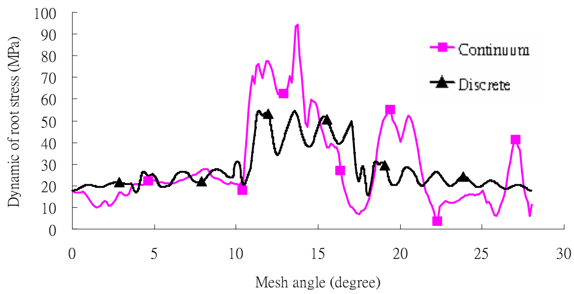

(b)

Figure 8. Comparison of fillet stresses of the planetary gear system using the both approaches: (a) fillet stresses on the sun gear for an external gear pair (b) fillet stresses on a planetary gear for an internal gear pair.

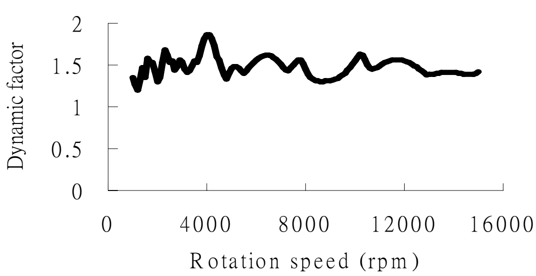

Figure 9. Dynamic factor of an external gear pair using the discrete approach.

5 CONCLUSIONS

Two dynamic approaches to a planetary spur gear system have been proposed, which are respectively using a conventional discrete model of the equivalent mass-damping-spring components and using a continuous geometry model by the finite element method. For the discrete one, the time varying meshing stiffnesses of gear pairs are considered by concerning the numbers, positions, and phasing angles of meshing tooth pairs beforehand. The natural frequencies, deformations, meshing forces, fillet stresses, and dynamic factors have been calculated. In the continuum aspect, dynamic responses of the planetary gear system have been analyzed using the FEM software, LS-DYNA. In contrast to the discrete model, this approach of continuous geometry model can incorporate the time varying characteristics intrinsically. Not using CAD models, the mesh elements of high quality for the planetary gear system are automatically generated directly using the derived tooth profile equations. Then, dynamic responses for the planetary gear system are also solved using the continuous model. Finally, both the results from the two approaches are verified by each other comparison. Using this continuum method, it is expected that the complicated and subtle dynamic analyses of planetary gear systems may be accomplished through the sophisticated descriptions. Not only the broad types of structure configurations, gears, or tooth profiles are, but also the complete coverage of influence factors is, such as the design parameter, backlash, tooth modification, and manufacturing error.

6 ACKNOWLEDGEMENTS

The authors would like to acknowledge the finical supports from National Science Council under grant of NSC-95-2221-E-216-008 and Chu Hua University under grant of CHU-95-2221-E-216-008. The software support from National Center for High Performance Computing is also acknowledged.

7 REFERENCES

[1] Botman, M., 1976, “Epicyclic Gear Vibration,” *ASME J. Eng. Ind.*, **17**, pp. 811-815.

[2] August, R., and Kasuba, R., 1986, “Torsional Vibrations and Dynamic Loads in a Basic Planetary Gear System,” *ASME J. Vib., Acoust. Stress Reliab. Des.*, **108**, pp. 348-352.

[3] Velex, P., and Flamand, L., 1996, “Dynamic Response of Planetary Gear Trains to Mesh Parametric Excitations,” *ASME J. of Mech. Des.*, **118**, pp. 7-14.

[4] Kahraman, A., 1994, “Planetary Gear Train Dynamics, ” *ASME J. Mech. Des.*, **116**, pp. 713-720.

[5] Parker, R. B., 2000, “A Physical Explanation for the Effectiveness of Planet Phasing to Suppress Planetary Gear Vibration,” *J. Sound Vib.*, 236, pp. 561-573.

[6] Parker, R. G. and Lin, J. 2004, “Mesh Phasing Relationships in Planetary and Epicyclic Gears,” *ASME J. Mech. Des.*, **126**, pp. 365-370.

[7] Velex, P., and Famand, L., 1996, “Dynamic Response of Planetary Trains to Mesh Parametric Excitations,” *ASME J. Mech. Des.*, **118**, pp. 7-14.

[8] Sun, T., and Hu, H.Y., 2002, “Nonlinear Dynamics of a Planetary Gear System with Multiple Clearances,” *ASME J. Mech. Des.*, **38**, pp. 1371-1390.

[9] Lin, J., and Parker, R. G., 1999, “Analytical Characterization of the Unique Properties of Planetary Gear Free Vibration,” *ASME J. Mech. Des.*, **121**, pp. 316-321.

[10] Lin, J., and Parker, R. G., 1999, “Sensitivity of Planetary Gear Natural Frequencies and Vibration Modes to Model Parameters,” *J. Sound Vib.*, **228**, pp. 109-128.

[11] Huang, K. J., and Liu, T. S., 2000, “Dynamic Analysis of a Spur Gear by the Dynamic Stiffness Method,” *J. Sound Vib.*, **234**, pp. 311-329.

[12] Tsai, M. H., and Tsai, Y. C., 1997, “A method for calculating static transmission errors of plastic spur gears using FEM evaluation,” *Finite Elem. Anal. Des.*, **27**, pp. 345-357.

[13] Litvin, F. L., Lian, Q., and Kapelevich, A. L., 2000, ”Asymmetric modified spur gear drives: reduction of noise, localization of contact, simulation of meshing and stress analysis,” *Comput. Method Appl. M.*, **188**, pp. 363-390.

[14] Chen, Y. C., and Tsay, C. B. 2002, “Stress analysis of a helical gear set with localized bearing contact,” *Finite Elem. Anal. Des.*, **38**, pp. 707-723.

[15] Brauer, J., 2004, “A general finite element model of involute gears,” *Finite Elem. Anal. Des.*, **40**, pp. 1857-1872.

[16] Litvin, F. L., 2004, *Gear Geometry and Applied Theory*. New York: Cambridge U. published.

[17] Yuksel, C., and Kahraman, A., 2004, “Dynamic Tooth Loads of Planetary Gear Sets Having Tooth Profile wear,” *Mech. Mach. Theory*, **39**, pp. 695-715.

[18] Bajer, A., and Demkowicz, L., 2002, “Dynamic Contact/impact Problems, Energy Conservation, Planetary Gar Trains,” *Comput. Method Appl. M.*, **191**, pp. 4159-4191.

[19] Litvin, F. L., Vecchiato, D., Demenego, A., Karedes, E., Hansen, B., and Handschuh, R., 2002, “Design of One Stage Gear Train with Improved Conditions of Load Distribution and Reduced Transmission Errors,” *ASME J. Mech. Des.*, **124**, pp.745-751.

[20] Parker, R.G., Agashe, V., and Vijayakar, S. M., 2000, “Dynamic Response of a Planetary Gear System using a Finite Element/Contact Mechanics Model,” *ASME J. Mech. Des.*, **122**, pp. 304-310.

[21] Liang, C. C., 2006, “Dynamic load Analysis of Planetary Gear Systems,” M.S Thesis, Chung Hua University, Taiwan (in Chinese).

[22] Kuang, J. H., and Yu, J., 1994, “A Dynamic Tooth Load Model of Addendum Modified Gear Pair,” *1994 ASME Design Technical Conferences*, DE-71, pp. 165-176.

[23] LSTC Ltd., 2003, LS-DYNA 970 Help Manual.

出席國際學術會議心得報告

計畫編號	NSC 95-2221-E-216-008
計畫名稱	以時變模式之行星齒輪系動態分析
出國人員姓名 服務機關及職稱	黃國饒（中華大學機械系副教授）
會議時間地點	96, 9/4 – 96, 9/7，美國 Las Vegas
會議名稱	2007 ASME International Design Engineering Technical Conferences (IDETC)
發表論文題目	Time Varying Approaches to Dynamic Analysis of a Planetary Gear System Using a Discrete and a Continuous Models

一、參加會議經過

- 9/4 下午(台灣時間) 至台灣桃園機場搭 CI-006 飛往美國 Las Vegas。
- 9/4 傍晚 (美國時間) 晚到達美國 Las Vegas。
- 9/5- 9/7 (美國時間) 全程參加 IDETC 2007，共聆聽了約 50 篇之論文發表，並提問討論。
- 9/5, 14:00-15:30 (美國時間) 進行本次發表之論文宣讀約 18 分鐘。
- 9/5, 20:00 (美國時間) 參與歡迎酒會，與各地相關研究學者討論交流。
- 9/5, 20:00 (美國時間) 參加 PTG 之晚宴，並與日本之齒輪研究學者進行討論交流。
- 9/7 晚上 (美國時間) 至 Las Vegas Mccarran 機場搭機返台。
- 9/9 早上(台灣時間) 抵台。

二、與會心得

此次為本人首次參加於國外舉辦之大型國際學術研討會，收穫極為豐碩，增加國際視野與個人研究信心。本屆 IDETC 2007 之 10th International Power Transmission and Gearing Conference (PTG)中，共有齒輪與傳動系統之研究論文共約 150 篇論文，主要包含 Design and Analysis, Dynamics and Noise, Strength and Durability 之領域論文為最多。本人此次發表之論文為提出關於行星齒輪系統之動態分析方法，將可以應用於廣泛行星齒輪系統之動態研究與設計應用，口頭報告結束後並與現場提問者交流討論。此外全程參與研討會各分組之論文發表，共聆聽

了約 50 篇之論文發表，主要為 Design and Analysis, Dynamics and Noise, Strength and Durability, manufacturing 相關研究為主，並與論文發表者進行交談，討論到關於如螺旋齒輪對應力分析、齒輪摩擦力量測、齒輪潤滑實驗、非線性動態模式、行星齒輪系統之非線性動態模式與響應等課題。會議中場休息以及用餐時間，本人也盡量主動與各國與會學者交談，進行廣泛交流。在此次首次參加國外之大型國際研討會，雖然在美時間只有三天，收穫感觸皆多。

個人認為，在未來齒輪系統之發展仍有無限發展的可能，包括更高轉速，更精密的傳動，更長的壽命以及更可靠的運轉。隨著當今環境保護與永續能源之發展，中華大學位於新竹應有所投注，尤其關於**大型風力發電系統用齒輪系統之發展**，包括更大發電容量、振動噪音防治、可靠度、系統整合之研究，建議隨著能源與環保之議題之趨勢，臺灣之產業發展彰顯特色與永續經營考慮時，此領域是特別值得注意投入的。。